Shahrood University of Technology

Journal of Mining and Environment (JME)

Journal homepage: www.jme.shahroodut.ac.ir

Iranian Society of Mining Engineering (IRSME)

Mineral Chemistry of the Gowd-e-Howz Granitoid Stock, SE, Iran: mineralization potential in relation to tectonomagmatic setting

Mahbubeh Arabzadeh Bani Asadi[1], Habibollah Ghasemi*[1], Mehdi Rezaei kahkhaei[1], Lambrini Papadopoulou[2]

1. Faculty of Earthscience, Shahrood University of Technology,Shahrood, Iran
2. Department of Mineralogy-Petrology-Economic Geology, School of Geology, AUTh, GR 54124 Thessaloniki, Greece

Article Info

Received 5 February 2025

Received in Revised form 21 April 2025

Accepted 26 May 2025

Published online 26 May 2025

DOI: 10.22044/jme.2025.15713.3020

Keywords

Geothermobarometry

Mineral chemistry

Granitoid

Gowd-e-Howz

Kerman, Iran

Abstract

The lower Jurassic (180 ± 1.5 Ma) Gowd-e-Howz granitoid stock, as a part of the Sanandaj-Sirjan Metamorphic-Magmatic Zone (SSMMZ), SE Iran, intruded in the Upper Paleozoic metamorphic and Triassic igneous-sedimentary rocks. It consists of three main rock units including diorite, granodiorite and granite/alkali feldspar granite, which accompanied by minor amounts of gabbro. The stock is predominantly composed of medium to coarse-grained granular granitoids consisting of clinopyroxene, amphibole, biotite, plagioclase, alkali feldspar and quartz. Clinopyroxenes exhibit calcic compositions, ranging from diopside to augite and salite, while amphiboles are primarily calcic with hornblende as the dominant phase. Feldspar display compositional ranges from orthoclase and oligoclase to labradorite. Mineralogical and geochemical evidence indicates this I-type calc-alkaline granitic magma produced in an active continental margin arc setting with potential for Cu-Au mineralization. Geothermobarometry estimations based on clinopyroxene (T= 800 to 1300°C and P= ~12 to 4.5 kbar), amphiboles (T= 742 to 769°C and P=4.5- 2 kbar) and biotite (T = 589 to 875°C and P= 0.45- 2.27 kbar), offer three different magma chamber levels for magma storaging and plumbing at the lower (~45 Km), middle (~16 Km) and upper (~5 Km) continental crust in an active continental arc setting in the Late Triassic-Early Jurassic in the southern part of the SSMMZ, SE Iran.

1. Introduction

Mineral chemistry of igneous rocks not only provides important information about nature of magma, its mineralization potential and tectonic setting [1-6], but also gives Key information about physicochemical conditions of crystallization, storaging and plumbing of magma systems [7-12].

The Gowd-e-Howz (Siah-Kuh) granitoid stock (180±1.5 Ma) is located in the southern part of the SSMMZ in the southeast of Kerman, South Iran (Figure 1). This stock represents the first magmatic product of subduction initiation in the Zagros Neotethyan realm at the Late Triassic-Early Jurassic [13-15]. Thus, the Gowd-e-Howz stock is one of the most important keys for understanding the subduction history of the Zagros Neotethyan oceanic basin beneath the Central Iran block. Despite some studies on petrology and whole-rock geochemistry of this stock [16, 14] and its related dikes [17], zircon U-Pb dating, mineral chemistries, mineralization potential and physico-chemical conditions of magma crystallization and emplacement are lacking and this paper provide the first insights into these issues. Here the zircon U-Pb dates and chemical compositions of the main rock-forming minerals from the Gowd-e-Howz granitoid stock (clinopyroxene, orthopyroxene, amphibole, plagioclase, and biotite) used to determine the nature of magma, its mineralization potential, tectonic setting of magma genesis and physical conditions (T, P) of magma plumbing and storaging.

Corresponding author: h-ghasemi@shahroodut.ac.ir (H. Ghasemi)

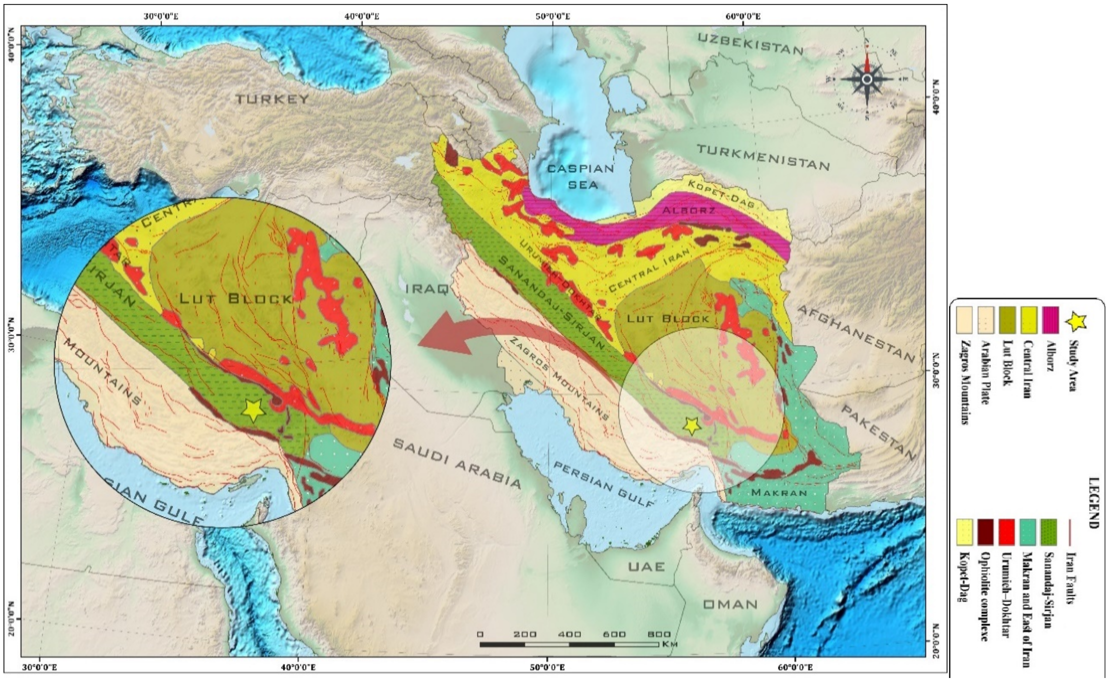

(a)

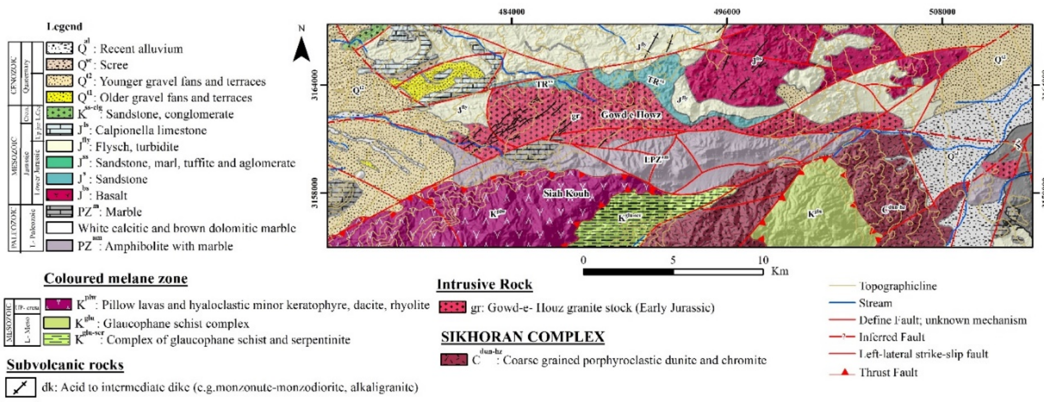

(b)

Figure 1. a) Position of the Gowd-e-Howz granitoid stock in the Sanandaj-Sirjan metamorphic-magmatic zone (SSMMZ), parallel to the Zagros orogenic belt (ZOB) in the structural map of Iran. b) Geological map of the Gowd-e-Howz granitoid stock based on new data of this research.

2. Geological setting

The Zagros Orogenic Belt (ZOBhich is locate) w d in the central part of the Alpine-Himalayan orogenic belt can be divided into five domains [18] including: (i) the Zagros fold-and-thrust belt, which extends ~2000 km from southeastern Turkey, through northern Syria and northeastern Iraq, to western and southern Iran; (ii) the Outer Zagros Ophiolitic Belt (OZOB) (Kermanshah–Neyriz–Hajiabad ophiolites) and associated HP/LT rocks [19-20], (iii) the SSMMZ, which extends as a NW–SE trending belt ~1500 km length and ~150–200 km width across south Iran; (iv) the Inner Zagros Ophiolitic Belt (IZOB) (Naein-Baft ophiolites), which extends for 500–600 km from Nain to Dehshir-Shahr-e Babak and Baft; and (vi) the Urumieh–Dokhtar magmatic arc (UDMA) with 50–80 km width composed of magmatic rocks formed by NE-dipping subduction of the Neo-Tethyan oceanic lithosphere beneath the Central Iran block during the Cenozoic (Figure 1).

The SSMMZ is a belt with 100–150 km width and extends approximately 1500 km from the Bitlis area in Turkey to the western end of Makran, SE Iran [19, 21-25]. This zone was undergone multiple phases of metamorphism and deformation and is composed of a variety of magmatic, metamorphic, and sedimentary rocks belong to the Late Neoproterozoic to Neogene [19, 24, 26-29]. These rocks were formed through a complex tectono-magmatic evolution resulting from initiation of the

Late Carboniferous rifting, Late Paleozoic-Mesozoic oceanic spreading, Mesozoic multiphase subduction (Late Triassic, Jurassic and Late Cretaceous) and the eventual closuring and colliding during the Cenozoic [15, 24, 30]. Extensive exposures of metamorphic rocks (metacarbonate, slate-phyllite-schist, gneiss, amphibolite, glaucophane schist and eclogite) in the SSMMZ distinguishes it from other Iranian geo-structural zones [31].

The SSMMZ has various metamorphic and magmatic rocks belonging to the Late Neoproterozoic to Mesozoic [24, 30-33]. The Late Neoproterozoic metamorphic rocks (mainly schist, gneiss and amphibolite) belong to the Central Iran continental basement, but the upper Paleozoic metamorphic rocks consist of medium to high temperature- low pressure rift type metamorphics (marble, schist, gneiss, and amphibolite) [30, 34-35]. The Mesozoic metamorphic rocks, as the main constituting rocks of this zone include (i) the Upper Triassic-Lower Jurassic slate-phyllite-schist, amphibolite and marble [30, 33-36], (ii) the Lower-Middle Jurassic amphibolite, migmatite, eclogite [19] and various schists, phyllites and slates of the Hamedan metamorphic complex [37], and (iii) the Upper Cretaceous blueschists [20, 34-36]. The metamorphic rocks of the SSMMZ were intruded by gabbroic to granitic plutons since Late Paleozoic through Mesozoic to Eocene [14, 19, 21, 30, 38].

3. Field and petrographic observations

The Gowd-e-Howz granitoid stock was intruded in the Upper Paleozoic Sargaz-Abshour metamorphic complexes (mainly composed of amphibolite, schist and marble, Figure 1 and 2a, b) and the Triassic igneous-sedimentary rocks (Figure1). The Lower Jurassic rocks mainly composed of conglomerate, sandstone, siltstone, shale and fossiliferous dark thin layered limestone and the Lower Cretaceous thick beded limestone covered the Triassic rock units and there isn’t evidence of granite intrusion in the Jurassic and Cretaceous rock sequences.

The Gowd-e-Howz complex stock has normal compositional zoning of the granitoids involving of the intermediate suites in the margins and the middle parts and the felsic suites in the central part. The stock mainly composed of granodiorite but it has a variety of rocks including minor amount of gabbro, diorite, quartz diorite, quartz monzonite, monzodiorite, monzonite, granodiorite, granite/alkali feldspar granite along with aplitic/pegmatite veins. Based on the field observations, the first phase of magma injection in the margins was of diorite type, which display dark color and contains diorite, quartz diorite, quartz monzonite and monzonite (Figure 2c, d). The second phase of magma emplacement was the intrusion of granodiorite into the diorites and made of the main part of the Gowd-e-Howz complex stock. The granodiorite is gray and has dark mafic microgranular enclaves [39] or mafic microgranitoid enclaves (MMEs) [40] with diorite, monzodiorite to monzonite compositions (Figure 2e, f). The existence of MMEs in the stock indicates the subsequent injection of the granodiorite phase into the first diorite phase. The third phase is a gray to pink, coarse-grained granite/alkali granite phase that intruded into the second granodiorite phase. It contains granodioritic enclaves and traces of Cu-Au mineralized veins and veinlets (Figure 2g-j). Finally, the middle Jurassic quartz monzonite dikes cut the whole of the Gowd-e-Howz granitoid stock and Lower Jurassic rocks and terminated into the Middle Jurassic dacitic-rhyolitic lava flows (Figures 1 and 2a).

3.1. Diorites

These rocks have fine to coarse-grained granular textures with very fine grained to inter-granular textures in the margins. The diorites contain orthopyroxene, clinopyroxene, plagioclase, hornblende and rarely biotite (Figure 3a). Minor minerals are opaque, apatite, titanite and alkali feldspar. The secondary minerals are serpentine, tremolite/actinolite, calcite, epidote, chlorite, sericite and clays. It seems that tremolite/actinolite formed by retrograde alteration of pyroxenes. Some hornblendes have replaced by the biotite along their margins and cleavages due to latter potassic alteration. The evidence of magma mixing/mingling process are also seen in the thin sections as the presence of dark fine-grained parts (MMEs), rich in amphibole and pyroxene in the lighter coarse-grained parts, rich in feldspar. Differentiated vein rocks of quartz diorite/monzonite have a fine, medium to coarse grained texture consisting of the main minerals of plagioclase, alkali feldspar, amphibole, and minor minerals of biotite, quartz, zircon, apatite, opaque and secondary minerals of calcite, quartz, epidote, chlorite and sericite.

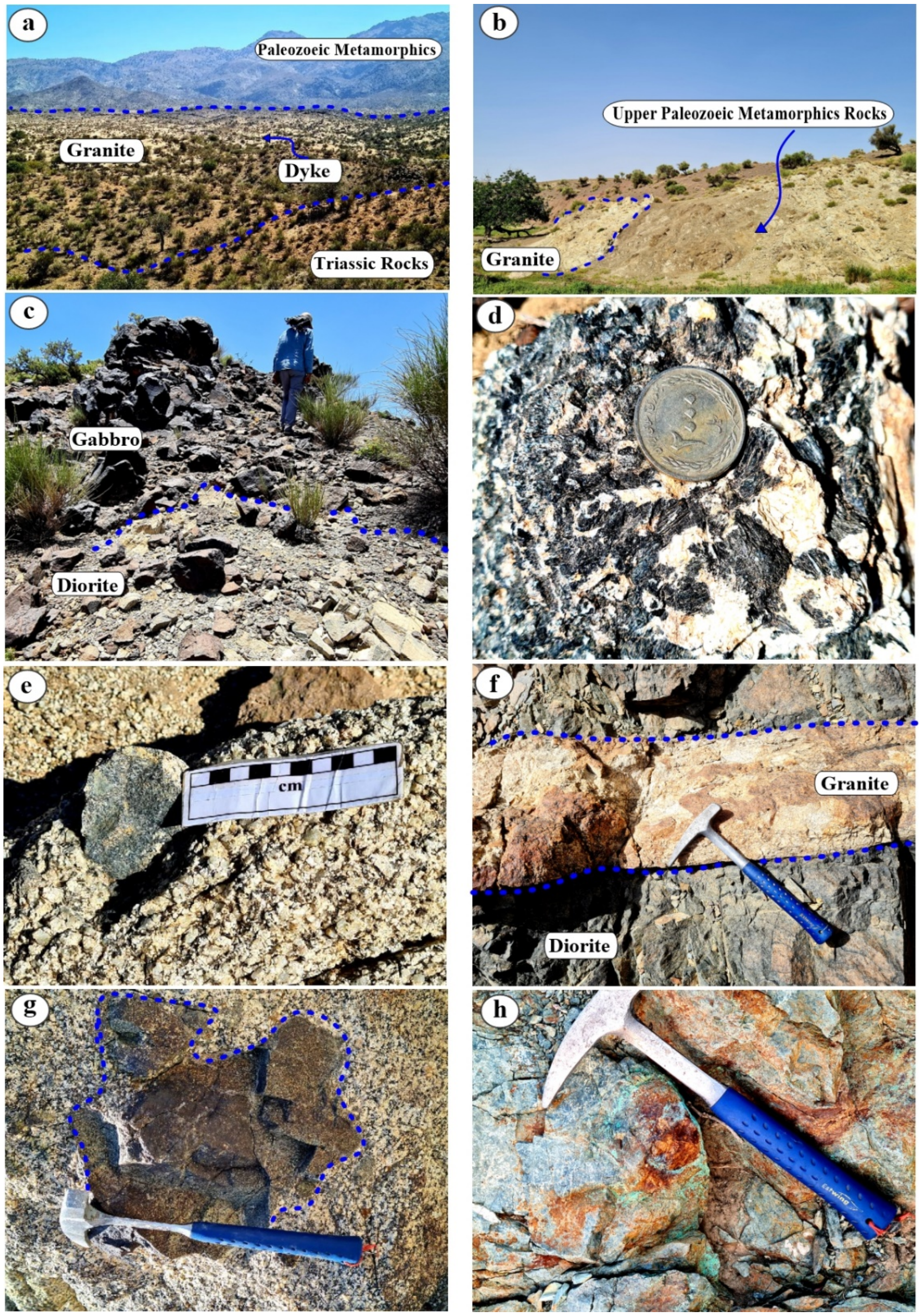

Figure 2. Field photographs from the Gowd-e-Howz granitoid stock and host rocks. a) Intrusion of the stock in the Upper Paleozoic metamorphic rocks in the southern and in the Triassic rocks in the northern border. b) Closed view of intrusive contact of the granitoid with the Upper Paleozoic metamorphic rocks. c) View of dark gabbroic and light dioritc parts of the stock. d) Closed view of pegmatitic structure of dioritc part composed of amphibole and plagioclase. e) Existence of dioritic enclave in granodiorite part. f) Intrusion of the granitic phase into the diorite part. g) Existence of granodioritic enclave in granite part. h) Closed view of Cu mineralization (malachite) in the granitic part.

3.2. Granodiorite

Granodiorites normally have coarse-grained anhedral granular texture, and sometimes shows micrographic and anti-perthitic textures. The main minerals are amphibole, biotite, plagioclase, quartz and alkali feldspar (Figure 3b). The minor minerals are apatite, zircon, and opaque, and secondary minerals include sericite, chlorite, epidote and clays.

3.3. Granites/alkali feldspar granites

Granites generally have coarse-grained granular texture (Figure 3c). Sometimes perthitic, micogranophyric, micrographic and myrmekitic textures found in theirs fractionated parts. Alkali feldspar granites mainly include aplite and pegmatite dykes, veins and veinlets, which have granular, micogranophyric, micrographic, myrmekitic, perthitic and poikilitic textures. Their main minerals include quartz, alkali feldspar, plagioclase, biotite and muscovite, minor minerals are zircon, apatite and opaque minerals, and secondary minerals include chlorite, epidote, calcite and clays. Quartz, alkali feldspar and plagioclase were formed very beautiful micrographic, worm-like myrmekitic and microgranophyric textures (Figure 3d), resulted by rapid simultaneous intergrowth of these minerals in a shallow depth [41].

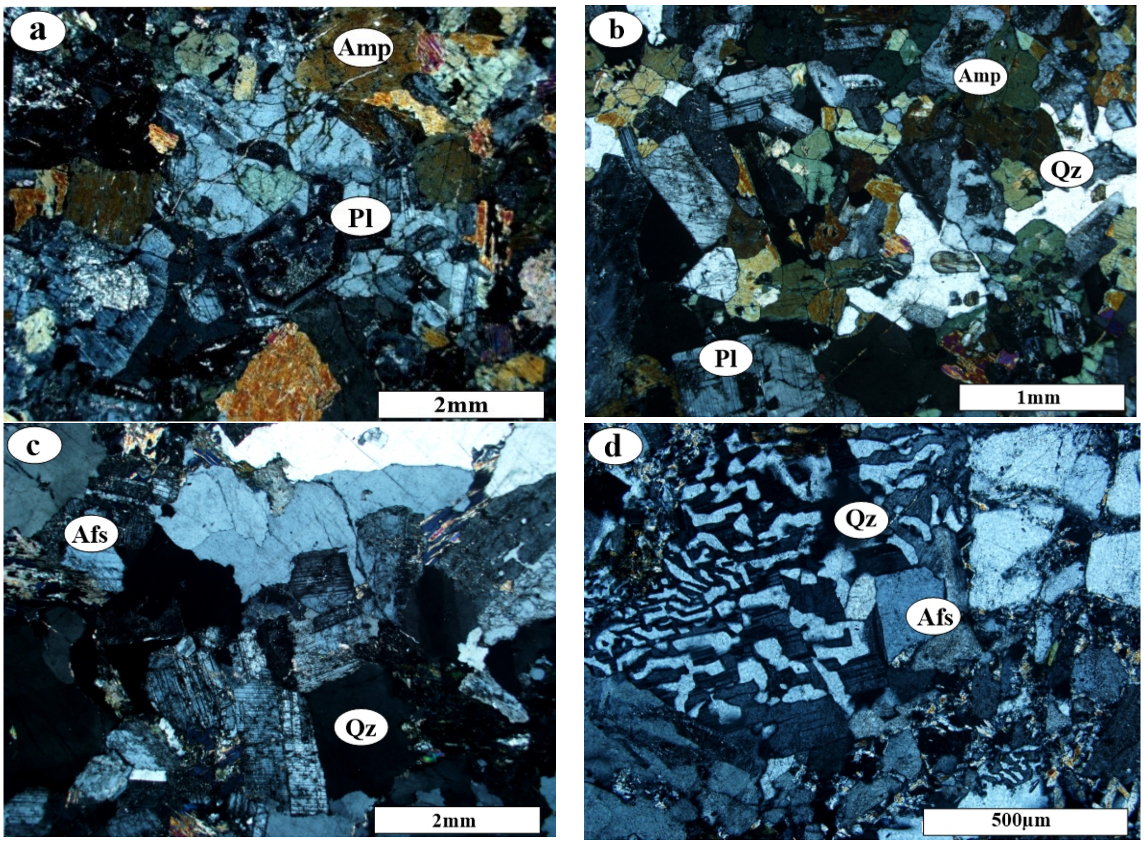

Figure 3. Photomicrographs of the rock units of the Gowd-e-Howz granitoid in the XPL light. a. Anhedral granular texture composed of amphibole (Amp), and plagioclase (Pl) in diorites. b. Anhedral granular texture composed of amphibole (Amp), plagioclase (Pl) and quartz (Qtz) in the granodiorites. c. Anhedral granular texture composed of alkali feldspar (Afs) and quartz (Qtz) in the alkali feldspar granites. d. Micrographic texture composed of alkali feldspar (Afs) and quartz (Qtz) in the alkali feldspar granites.

4. Sample selection and analytical methods

4.1. Mineral Chemistry

A total of 200 samples have been collected from the Gowd-e-Howz granitoid stock, associated dikes and surrounding host rocks during field works. Thin and polished thin sections were prepared for petrographic studies and microprobe analysis in the labs of the Faculty of Earth Sciences, Shahrood University of Technology, Shahrood, Iran. Thirteen samples from diorites, granodiorites and granites selected for mineral chemistry analysis and more than 900 points have been analyzed. The in-situ analyses of minerals on five samples (MH-6, MH-8, MH-21, MH-40 and MH-43) were carried out at the GFZ Potsdam (Germany) using a JEOL-JXA 8230 microprobe equipped with five WDS. The operating conditions were as follows: 15kV accelerating voltage, 20nA beam current and 10s counting time on peak position for Si, K, Cr, Na, P or 20 s counting time for Al, Ca, Fe, Mn, Mg, Ti, F, Cl. Detection limits are 0.02–0.9 wt%.

The microprobe analyses of eight samples (MH-6, MH-43, MH-51, MH-53, MH-56, MH-57, MH-58 and MH-66) conducted using a JEOL JSM-6390LV scanning electron microscope (SEM), at the Aristotle University of Thessaloniki, Greece. The operating conditions were a 20kV accelerating voltage and 0.4 mA probe current, 80s counting time, and a beam diameter of 1 µm. The samples coated with carbon– average thickness of 200 Å- using a vacuum evaporator JEOL-4X.

The cation numbers of the pyroxenes, feldspars, amphiboles and biotites were calculated with an excel spreadsheet based on 6, 8, 23 and 22 Oxygen, respectively. Fe^{3+} content calculated in pyroxenes according to [42] and in amphiboles according to [43]. The data has been processed with specialized soft wares of Geo-fO_2 [8], WinAmptb [44], WinPyrox [45, 46] and excel spreadsheets such as Amp-TB2.xlsx [10] and the graphs have been drawn by the Grapher software.

4.2. U-Pb dating

Two granodiorite samples (MH-1 and MH-21) from the Gowd-e-Howz granitoid stock selected for SHRIMP zircon U-Pb dating. Zircons were separated using panning, first in water and then in ethanol. This was followed by magnetic extraction of Fe-rich minerals with a Nd magnet. Finally, zircons handpicked using a binocular microscope. The zircons cast on "megamounts", i.e., 35 mm epoxy discs fixed on the front of a mount holder so that no metallic parts or surface discontinuities faced the secondary ions extraction plate. The minerals were carefully studied with optical (reflected and transmitted light) and scanning electronic microscopy (backscattering and cathodoluminescence) prior to SHRIMP analyses with the IBERSIMS SHRIMP IIe/mc ion microprobe at the IBERSIMS laboratory, University of Granada, Spain. Zircons analyzed for U-Th-Pb following the method of [47]. The mount coated with a ≈12 nm thick gold layer. Each spot was rastered with the primary beam for 120s prior to analysis and then analyzed for 6 scans following the isotope peak sequence $^{196}Zr_2O$, ^{204}Pb, 204.1 background, ^{206}Pb, ^{207}Pb, ^{208}Pb, ^{238}U, ^{248}ThO, ^{254}U.

Every peak of every scan was measured sequentially 10 times with the following total counting times per scan: 2s for mass 196; 5s for masses 238, 248, and 254; 15s for masses 204, 206, and 208; and 20s for mass 207. The primary beam, composed of 16O-16O+, was set to an intensity of about 5nA, with a 120 microns Kohler aperture, which generated 17 x 20 micron elliptical spots on the target. The secondary beam exit slit was fixed at 80 microns, achieving a resolution of about 5000 at 1% peak height. All calibration procedures were performed on the standards included on the same mount. Mass calibration was done on the REG zircon (ca. 2.5 Ga, very high U, Th and common lead content). The analytical session started by measuring the SL13 zircon [48], which used as a concentration standard (238 ppm U). The TEMORA zircon (416.8 ± 1.1 Ma) [49], used as an isotope ratios standard, was then measured every four unknowns. Data reduction was done with the SHRIMPTOOLS software (available from www.ugr.es/~fbea), which is a new implementation of the PRAWN software originally developed for the SHRIMP. Errors reported at the 95% confidence interval (≈2 σ). Standard errors (95% C.I) on the 37 replicates of the TEMORA standard measured during the analytical session were 0.18 % for $^{206}Pb/^{238}U$, and 0.62 % for $^{207}Pb/^{206}Pb$.

5. Results

5.1. Mineral chemistry

The chemical compositions of rock-forming minerals in the Gowd-e-Howz granitoid stock as a reflection of its constituent magma composition provide valuable tools to evaluate source and nature of magma and its mineralization potential [1, 3, 5-6], tectonic setting of magma genesis [2, 4-5, 50] and physico-chemical conditions of magma crystallization, storaging and plumbing (P, T) [8-12, 51-71].

5.1.1. Pyroxenes

Diorites and minor gabbroic parts of the Gowd-e-Howz granitoid stock contain pyroxenes (usually clinopyroxenes and rarely orthopyroxenes). The orthopyroxenes have high Mg/Fe and low Ca contents and plot mainly in the field of magnesium pigeonite in gabbros ($En_{59–81}Fs_{17–34}Wo_{0.70–3.35}$) and intermediate pigeonite in diorites (Table 1 and Figure 4b). The clinopyroxenes have different compositions (Table 2) and plot in the fields of diopside-augite-salite ($En_{34–56}Fs_{04–18}Wo_{36–51}$) in the pyroxene classification diagram [42] (Figure 4b). The compositional ranges of clinopyroxenes show variations between diopside-augite-Mg augite (in gabbros) to salite (in diorites) (Figure 4b).

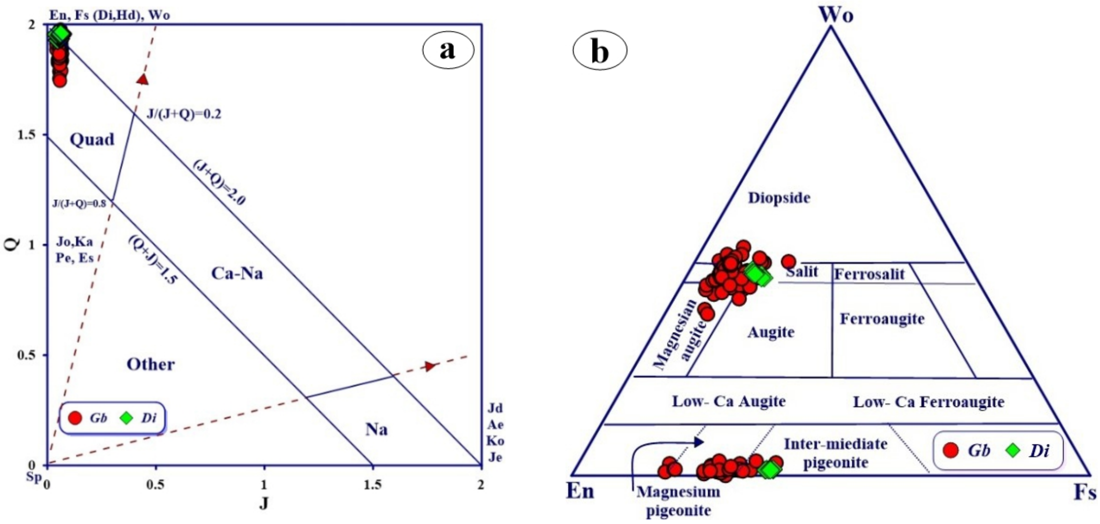

Figure 4. Composition of analyzed pyroxenes from the Gabbro and diorite samples of the Gowd-e-Howz granitoid stock on the: a) J-Q classification diagram from [42] in the field of Quand and, b) En-Fs-Wo diagram from [42] in the fields of diopside-augite-salite and magnesium pigeonite to intermediate pigeonite.

5.1.2. Amphiboles

The study amphiboles are calcic and characterized by a large range of Mg# [Mg/(Mg+Fe^{2+}) and TSi between 6.50-7.97 a.p.f.u, (Table 3) classification diagrams [43] plot in the fields of magnesium hornblende-tschermakite hornblende (in gabbros), magnesium hornblende-tschermakite hornblende-tremolite hornblende (in diorites) and magnesium hornblende-tschermakite hornblende-ferro tschermakite-ferro tschermakite hornblende-ferro hornblende to tremolite-actinolite (in granodiorite/granites)(Figure 5a-e). Amphiboles with tremolite-actinolite compositions found in granodiorite/granites is post magmatic with secondary origin probably formed by retrograde alteration of clinopyroxenes. The calcic amphiboles normally are indicators of I-type granitoids [72]. In the Ca+Na+K versus Si diagram [73] which separates igneous and metamorphic amphiboles, the Gowd-e-Howz amphiboles plot in the field of igneous type (Figure 5f).

5.1.3. Feldspars

The feldspars of the Gowd-e-Howz granitoid samples have variable main oxide contents ranging SiO_2 from 41.20– 68.45 wt%, CaO from 0.07–20.11 wt%, Na_2O from 0.02–11.75 wt%, K_2O from 0.00–16.60 wt%, and Al_2O_3 from 18.37– 37.89 wt% (Table 4). In the Ab-Or-An feldspar classification ternary diagram [77], the analyzed plagioclase is ranged 74 – 98 An% (bytonite-anorthite) in the gabbros, 1 – 81 An% (albite-bytonite) in the diorites, and 1 – 61 An% (albite-labradorite) in the granodiorite/granites (Table 4). The K-feldspars from the alkali granites have relatively uniform compositions. They contain high orthoclase contents (> 98%) and lie in the field orthoclase on the feldspar classification diagram (Figure 6).

5.1.4. Biotites

The chemical composition of biotite is classically used to: (i) estimate the conditions and geotectonic setting of magma genesis, (ii) determining the oxygen fugacity during the magma crystallization [78-79], (iii) estimate the liquidus temperature of magmas [8, 80-81], (iv) genetic classification of the granitoids and theirs mineralization potential [4, 82-83] and (v) to date the thermal events and age of its host rocks. The composition of biotite in igneous rocks varies between the four end members of magnesium-bearing (phlogopite), iron-bearing (annite) and aluminum-bearing eastonite-siderophyllite (Figure 7); so that it is usually of phlogopite type in the gabbro and diorite and annite type in the granodiorite and granite) [84]. Biotites of the Gowd-e-Howz granitoid stock (table 5) have been plotted in the fields of primary and secondary biotites [83] (Figure 7) and iron-bearing biotites (Figures 7-b, c, d, e), which is consistent with their greenish-brown color in Plan Polarized Light (PPL) in thin sections.

Ternary diagram developed by [83] with [(10×TiO_2) – (FeO+MnO) – MgO] as coordinates was used to signify the primary or re-equilibrated nature of the biotites in the Gowd-e-Howz granitoid stock. In this diagram, although the biotites plotted in the primary magmatic field, but they placed on the side inclined to secondary biotites, which is consistent with the petrographic evidence of the K-alteration of some amphiboles to biotite. If the Al_{VI} content of biotite is <1 it denotes its primary magmatic origin [83], which is consistent with the studied biotites (0.04 – 0.16).

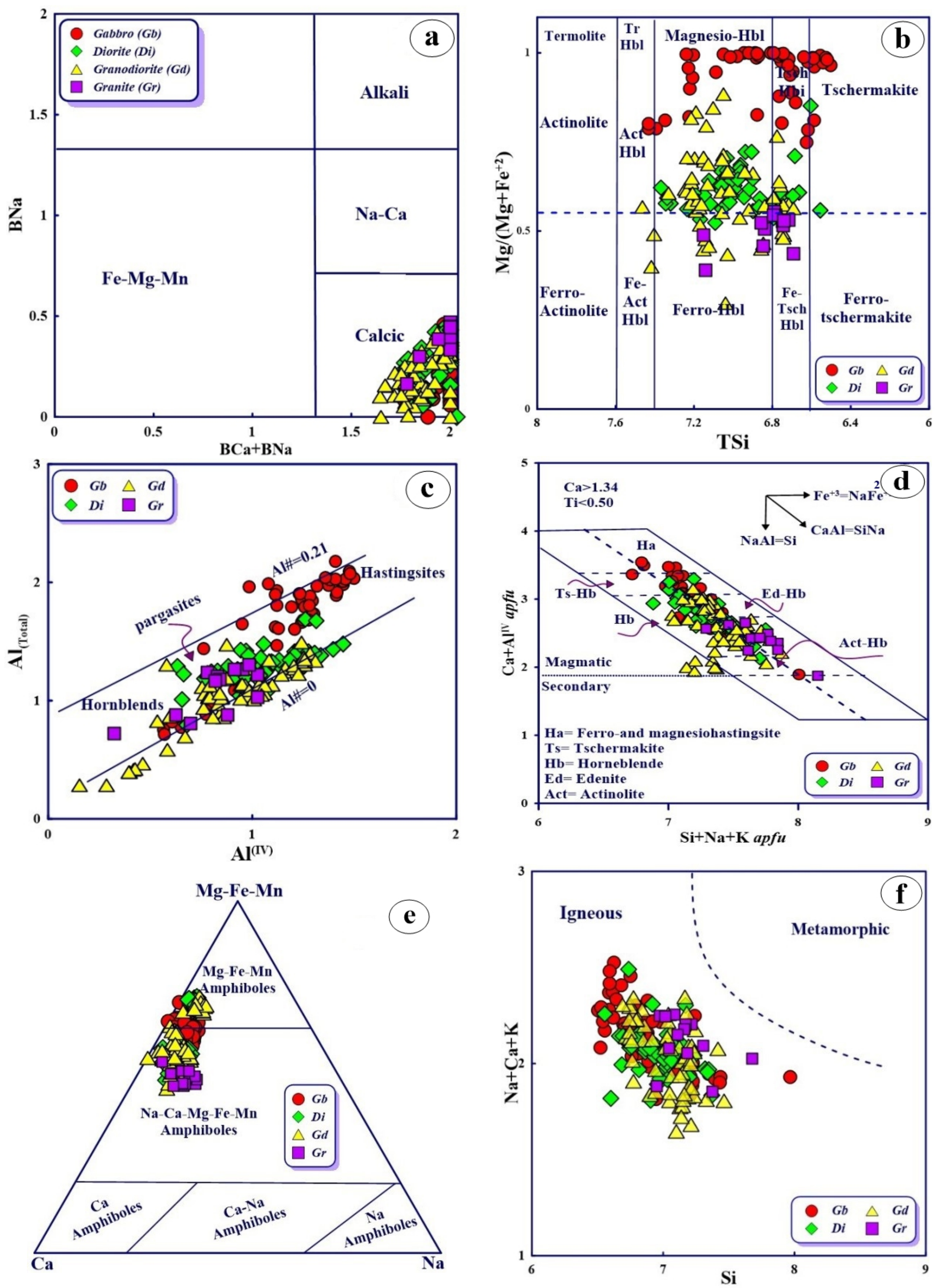

Figure 5. Composition of analyzed amphiboles in the gabbro, diorite and granodiorite/granite samples of the Gowd-e-Howz granitoid stock on classification diagrams: a) From [43]. b) From [74]. c) From [51]. d) From [75]. e) From [76]. f) From [73].

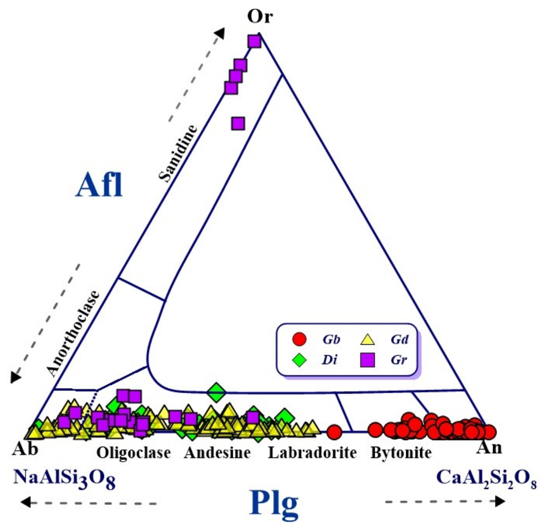

Figure 6. Plot of the Gowd-e-Howz granitoid feldspars in the Ab-Or-An ternary classification diagram from [77].

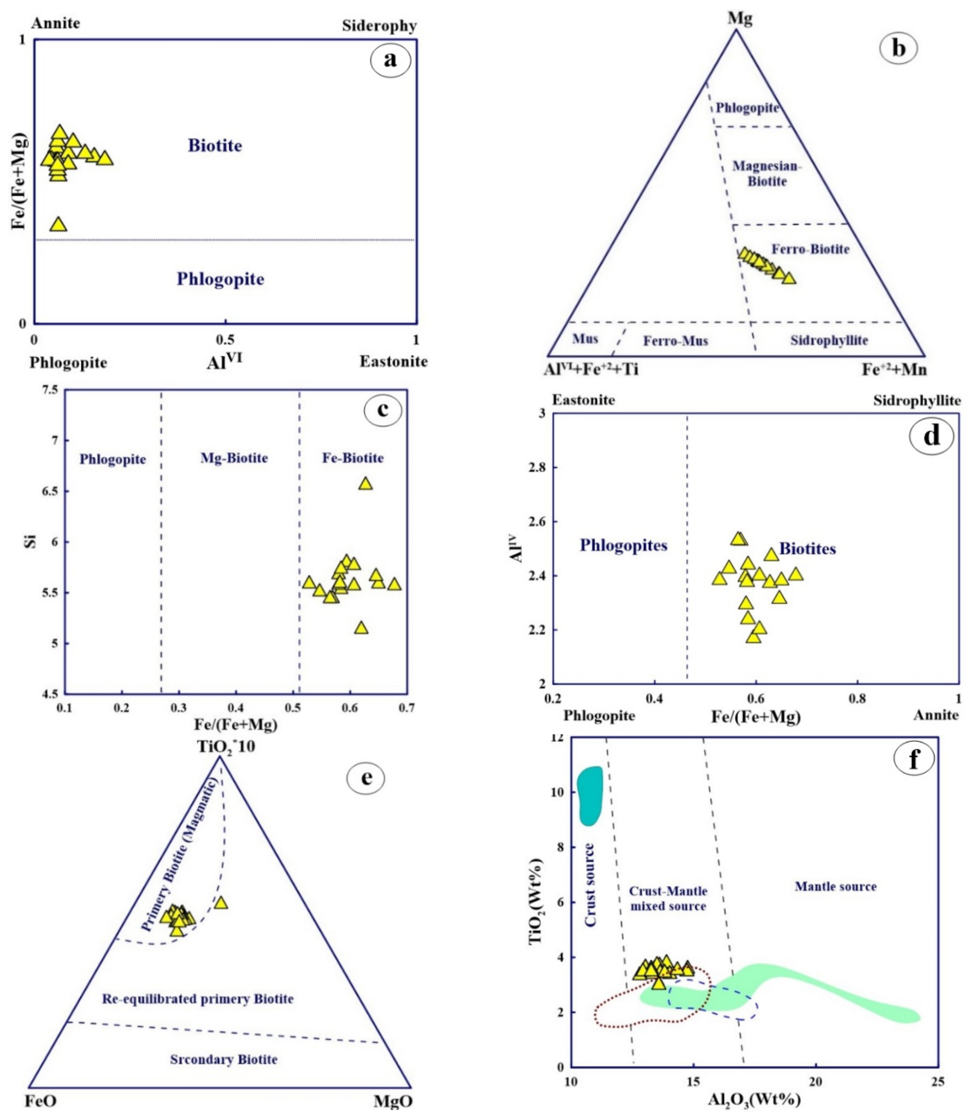

Figure 7. Plotts of biotites of the granodiorites from the Gowd-e-Howz granitoid stock in the different classification diagrams. a. From [77]. b. From [85]. c,d From [77]. e. From [83]. f. From [86].

6. Discussion

The mineral chemistry of pyroxene, amphibole, feldspar and biotite from different rock units of the Lower Jurassic Gowd-e-Howz granitoid stock have been analyzed for studying the detailed chemical composition of these minerals, nature of magma, it's mineralization potential and tectonic setting, and physical conditions of crystallization (T, P) during the final emplacement of the magma injection in the crust.

6.1. Crystallization conditions

6.1.1. Clinopyroxene geothermobarometry

Clinopyroxene geothermobarometers are the most commonly used mineral-based igneous thermobarometers, since this mineral is commonly present in a wide range of different magmatic rocks (ultramafic-mafic-intermediate) and tectonic settings (mid-oceanic ridges, oceanic islands, active continental margins, hot spots and rifts) and exhibits large compositional variations in each rock and environment setting [12, 45, 46, 62, 87]. Chemistry of clinopyroxene is sensitive to pressure and temperature of magma [11-12, 45-46, 50, 63, 70-71, 88-89, 90-92]. It is stable in a wide range of temperatures (800 to 1500ºC) and pressures (1 bar to 30 kbar) [7, 45]. Here, Excel spreadsheet [62] and WinPyrox software [92] used for thermobarometric calculation. Application of these thermobarometers for clinopyroxenes of the Gowd-e-Howz granitoid stock show the gabbros were crystallized at P= 1.16-7.71 kbar and T= 1030-1244ºC corresponding to the temperatures obtained by [46, 62, 93]. Moreover, the diorites were crystallized at P= 1.42-9.07 kbar and T= 1176-1184ºC (Table 2 and Table 6) and Figures 8.

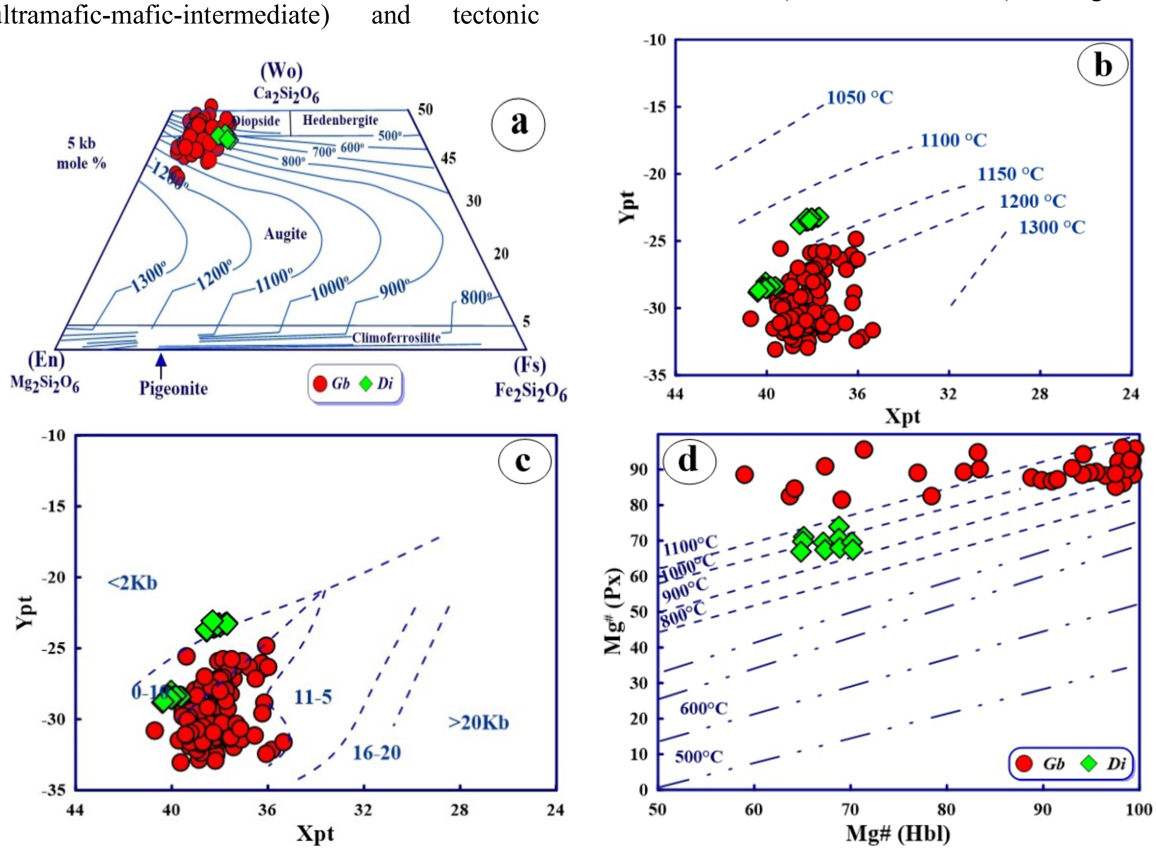

Figure 8. Temperature and pressure estimations of clinopyroxene crystallization in gabbro/diorite part of the Gowd-e-Howz granitoid body in the various diagrams. a. Estimation of temperature by [63] method. b. Estimation of temperature and c. pressure by [71] method. d. Plot of Mg≠ of hornblende versus Mg≠ of clinopyroxene from [51].

6.1.2. Two-feldspar geothermometry

The distribution of $NaAlSi_3O_8$ (albite content) between two coexisting solid solution phases recognized as a valuable geothermometric tool. The early calibrations based on binary exchange of albite component. Most recent offer three calibrations for each feldspar pair based on exchange of albite, anorthite and orthoclase components respectively [94]. Two co-existing feldspars in a rock strongly depend on temperature but less on pressure. In two-feldspar thermometry, the feldspars are characterized by component exchanges easily reset during slow cooling or later thermal events; only in shallow emplaced plutons two-feldspar thermometry yield consistent hyper solidus results [54]. Multi-thermobarometer excel sheet calculation prepared by [45] was applied here for estimating of T values obtained based on the equation given by [94]. The results gave in Table 4. The calculated T for the Gowd-e-Howz samples range from 512 to 750°C (Figure 9). Because of the low closing temperature of the feldspars, these low values are re-equilibration closing temperatures, completely differing from crystallization temperatures.

6.1.3. Amphibole geothermobarometry

Amphibole is an ideal mineral for evaluation of P-T conditions of calc-alkaline intrusions emplaced within orogenic belts, due to their diverse chemical composition and mineral structure. It observes in a wide range of temperature-pressure stability (P= 1-23 kbar and T= 400-1150°C). Here we used the different geobarometer equations of 1 from [59] with uncertainty range of ±3 kbars , 2 from [95] with uncertainty range of ±1 kbars, 3 from [61], with uncertainty range of ±1 kbars, 4 from [69], 5 from [53] with uncertainty range of ±0.6 kbars, and 6 from [65, 66].

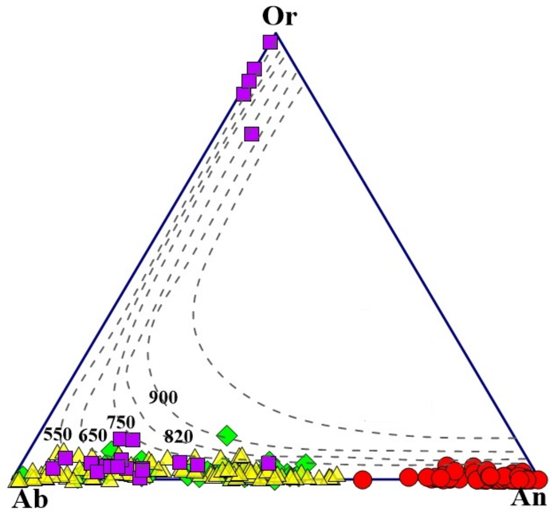

Figure 9. Plots of feldspar compositions of the Gowd-e-Howz granitoid stock on the Or-Ab-An ternary diagram [52] for determining the equilibrium closing temperatures of the feldspars.

$$P = -3.92 + 5.03\, Al^{tot} \quad (1)$$

$$P = -4.76 + 5.6\, Al^{tot} \quad (2)$$

$$P = -3.46 + 4.23\, Al^{tot} \quad (3)$$

$$P = -3.01 + 4.76\, Al^{tot} \quad (4)$$

$$P=-3.01+4.76\, Al^{tot}-\{T[°C]-675.85\}\times\{0.53\, Al^{tot}+0.005294\times(T[°C]-675)\} \quad (5)$$

$$P = 19.209 e^{1.483 Al^{tot}} \quad (6)$$

Applying these different methods to amphiboles of the gabbro from the Gowd-e-Howz granitoid stock represents P= 1.0-6.9 kabr and T= 647-948◦C, while this mineral in diorite represents P= 1.0- 6.9 kabr and T= 665-912°C (Tables 7 and 8).

Moreover, the diagram of tetrahedral aluminum (Al_{iv}) vs. octahedral aluminum (Al_{vi}) in amphibole structural formula [9] used to estimate pressures of amphibole crystallization. In these diagrams, amphiboles of the Gowd-e-Howz granitoid stock are plotted in the low-pressure range (Figure 10 a). The diagram of $Fe^{+2}/(Fe^{+2}+Mg)$=Fe≠ versus total aluminum ($Al^{VI}+Al^{IV}$) [69] applied to estimate pressure of amphibole formation (Figure 10 b). In this diagram, amphibole of the Gowd-e-Howz granitoid stock plot in the pressure ranges between 1 to 4 kbar.

Granodiorite and granite consist mainly of green hornblende and plagioclase, the required minerals for thermobarometry. Following equation [7] presented as an amphibole geothermometer:

$$T[°C]=1781-132.74\times Si_{Amph}+116.6\times Ti_{Amph}-69.41\times Fet_{Amph}+101.62\times Na_{Amph} \quad (7)$$

Applying this method for the amphiboles of the Gowd-e-Howz granitoid represents the temperatures ranges from 725-835°C for granodiorites and 632-884°C for the granites (Table 8). An Excel spreadsheet program, which operates within Microsoft Excel 10 [10], allows applicant to calculate the P (pressure) and T (temperature) conditions of steady-state magmatic crystallization of calcic amphiboles from its major elements composition (e.g. EPMA). Applying this method to amphiboles of the Gowd-e-Howz rocks gave the temperatures range from 623-944º C and 736-850ºC for granodiorites and granites, respectively (Table 8).

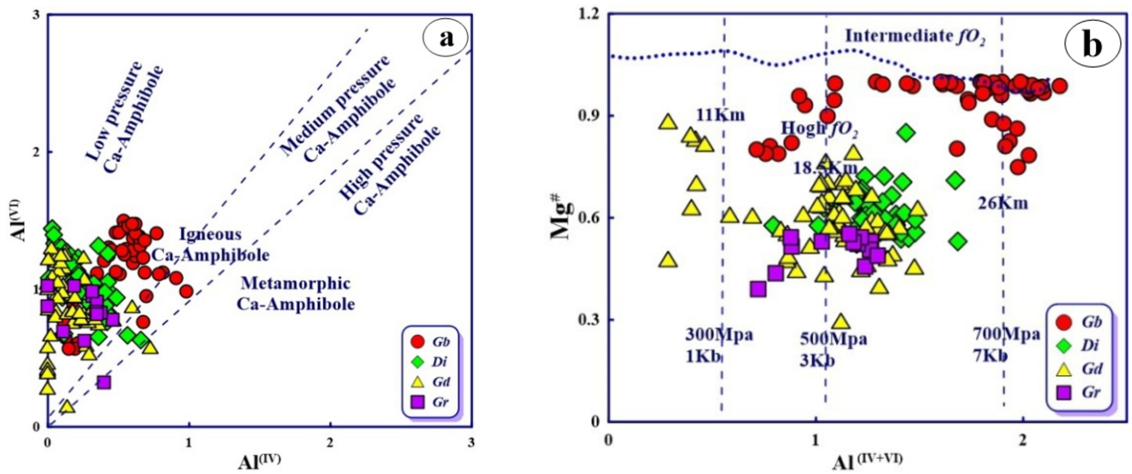

Figure 10. a. Plot of the Gowd-e-Howz granitoid amphiboles in the field of low-pressure amphiboles in diagram of tetrahedral aluminum (Aliv) vs. octahedral aluminum (Alvi) in amphibole structural formula from [9]. b. Plot of amphibole compositions of the Gowd-e-Howz granitoid stock on the diagram of Fe≠ vs. Al_{total} from [69].

The amphiboles of the Gowd-e-Howz granitoid stock plotted in a thermometric graph based on amounts of Al^{IV} versus Ti in amphiboles [57] (Figure 11a). They show temperature ranges of 650 to 900°C in this graph. Naturally, the higher temperatures are close to the crystallization temperatures and the lower ones correspond to the closing temperatures. The diagram of Ti versus (Na+K) from [68] also used as an amphibole thermometer for the Gowd-e-Howz granitoid stock, that shows the T values in ranges lower than 750°C (Figure 11b).

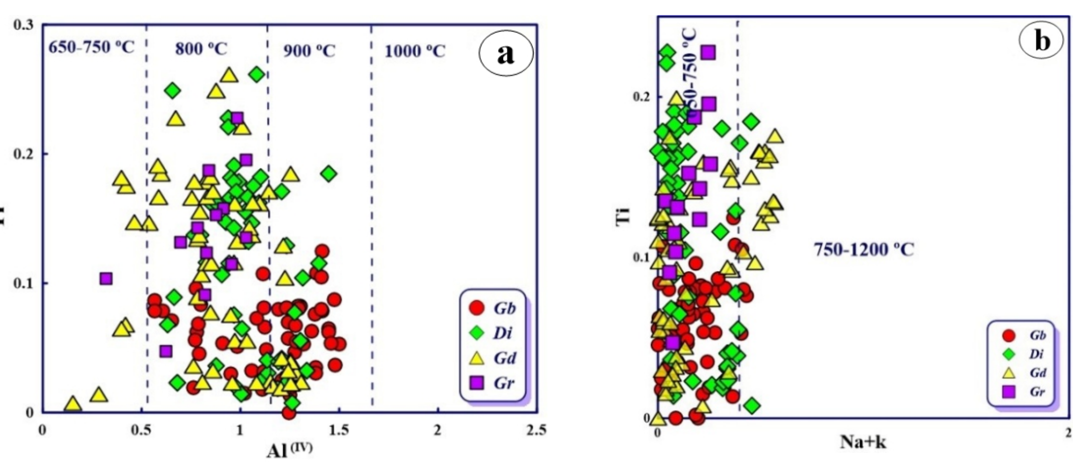

Figure 11. Plots of the Gowd-e-Howz granitoid amphiboles in the: a) graph of Al^{IV} vs. Ti in amphibole from [57] and, b) graph of Ti vs. (Na+K) from [68].

6.1.4. Biotite Geothermobarometry

The Ti content of biotite is sensitive to crystallization temperature of magma [96]. The empirical and experimental correlation between temperature, Ti, and Mg# =[Mg/(Mg + Fe^{2+})] of biotite (Ti-in-Biotite thermometer) was acknowledged by several authors [8, 81]. These authors by using a set of natural biotite compositions empirically calibrated the relationship between Ti, Mg#, and temperature of the biotite crystallization. The other empirical formula presented as follows [81]:

$$T = ([\ln(Ti) - a - c(X_{Mg})^3]/b)^{0.333} \qquad (8)$$

Where, a= -2.3594, b= 4.6482×10^{-9}, c= -1.728, and X_{Mg}= Mg/(Mg+ Fe^{2+}). This formula can only be applied to biotite bearing rocks, having X_{Mg}=0.275 - 1.00; Ti=0.04 - 0.60 (apfu). The uncertainty of the Ti-in-biotite geothermometer is estimated to be ±12ºC at lower temperatures (< 600ºC), improving to ±12°C at high temperature (>700°C) [81]. The estimated temperature based on [81] gives T= 689-751°C ±12ºC for the granodiorites from the Gowd-e-Howz stock (Figure 12). The crystallization pressure of biotites was calculated using empirical formula as follows [97]:

$$P(kb) = 3.03 \times Al^T - 6.53\ (\pm 0.33) \qquad (9)$$

The uncertainty of this formula is ±33 MPa. This geobarometric formula can only applied to biotite bearing rocks. The calculated pressure ranges from 0.74 to 4 ±0.3 kbar.

6.2. Identification of magmatic series and tectonic setting

The clinopyroxene composition refers to the nature of the host magma [98-99]. The clinopyroxenes of the Gowd-e-Howz samples contain high SiO_2 (>50 wt%) and relatively low Al_2O_3 (< 4 wt%) point to the subalkaline (calc-alkaline) nature of the parental magma [50] (Figure 13a). This subject also supported by plotting of the study clinopyroxenes in the sub-alkaline field of Al_2O_3 versus TiO_2 diagram [1] (Figure 13b).

The abundances of TiO_2 and Cr in the clinopyroxenes of the Gowd-e-Howz stock are low and they plot in the field of volcanic arc on a Ca versus Ti+Cr diagram [1] (Figure 13c). Clinopyroxene chemistry in the form of F1 and F2 parameters [50] used for discriminating the tectonic setting of magmatic rocks.

These parameters for the Gowd-e-Howz granitoid samples range between -0.36 to -0.46 and -2.35 to -2.26, respectively, and the study clinopyroxenes plot in the field of volcanic arc basaltic magmas (Figure 13d).

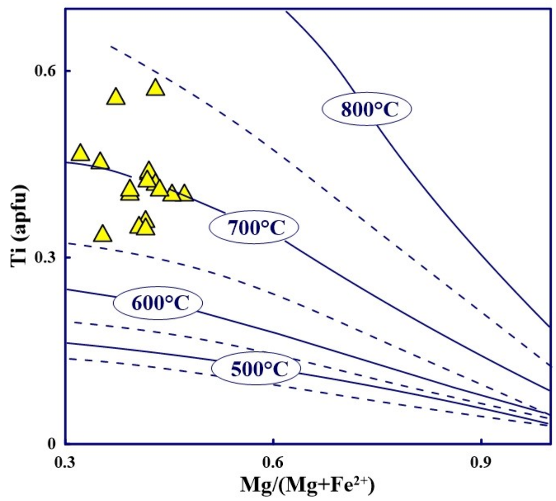

Figure 12. Plot of biotites of the Gowd-e-Howz granitoid stock in the Ti vs. Mg# diagram from [81] to estimate the crystallization temperatures of biotites.

The presence of calcic amphiboles in granitoid rocks indicates that these rocks belong to calc-alkaline I-type granitoids [72, 100], because the high amount of CaO in these granites, leads to the crystallization of hornblende. The participation of Mg, K and Ti in the amphibole structure depends on the nature of the magma, so that amphiboles of the sub-alkaline compared to the alkaline systems have lower amounts of Na_2O, TiO_2, K_2O and Al_2O_3 [6]. Compositions of amphiboles from the Gowd-e-Howz granitoid samples on bivariant discrimination diagrams of K_2O, Na_2O, Al_2O_3 and MgO versus TiO_2 [65, 67] confirm the sub-alkaline I-type nature of theirs parental magma (Figure 14a-d), supported also by clinopyroxene chemistry (Figure 13).

The chemistry of amphibole, especially the magnesium number (Mg#) of hornblende can used to determine the origin of magma. High values (>0.7) and low values (>0.5) of this number indicate mantle and crustal origins, respectively, and values between 0.5 and 0.7 indicate mixing with crustal sources. Amphiboles from the Gowd-e-Howz stock have Mg#= 0.5 - 0.7, indicating a mixing origin of crustal and mantle magmas (Figure 7f), confirmed by TiO_2 versus Al_2O_3 diagram [3] (Figure 15a). The value of TiO_2 in amphiboles from the Gowd-e-Howz granitoid is less than 2wt% and plot in the field of those amphiboles crystallized from the subduction zone magmas on the TiO_2 vs. SiO_2 diagram [5-6](Figure 15b, c).

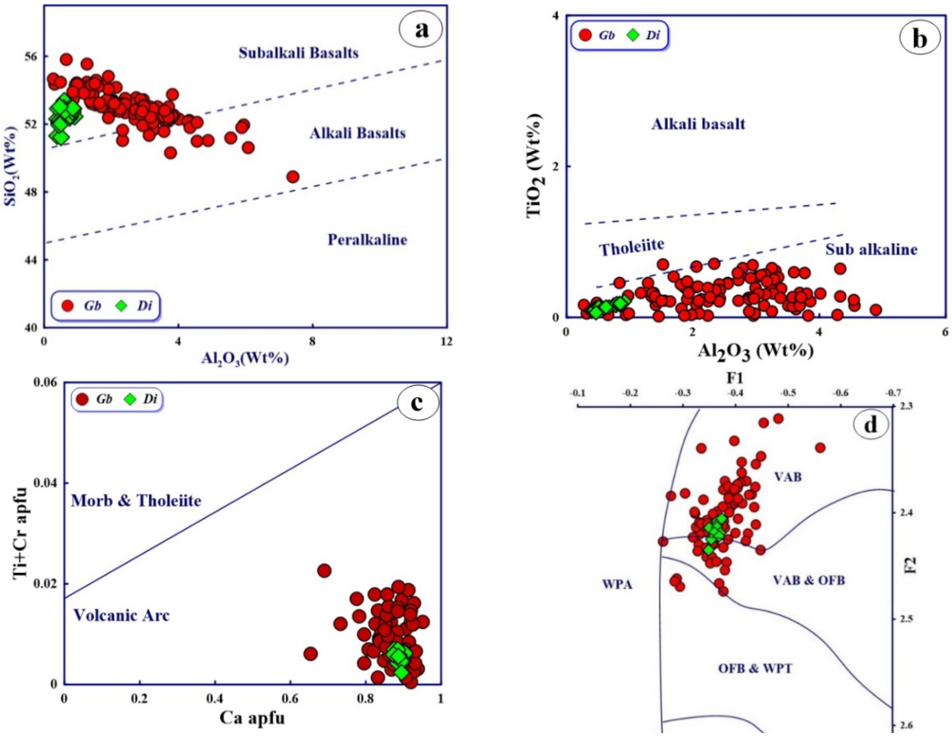

Figure13. Plots of clinopyroxene compositions of the Gowd-e-Howz granitoid stock on the field of the subalkaline magmas of volcanic arcs on the diagrams of: a) Al_2O_3 vs. SiO_2 from [50] and b) Al_2O_3 vs. TiO_2 from [1]. c) Ca versus Ti+Cr (from [2] and, d) F1-F2 diagram from [50].

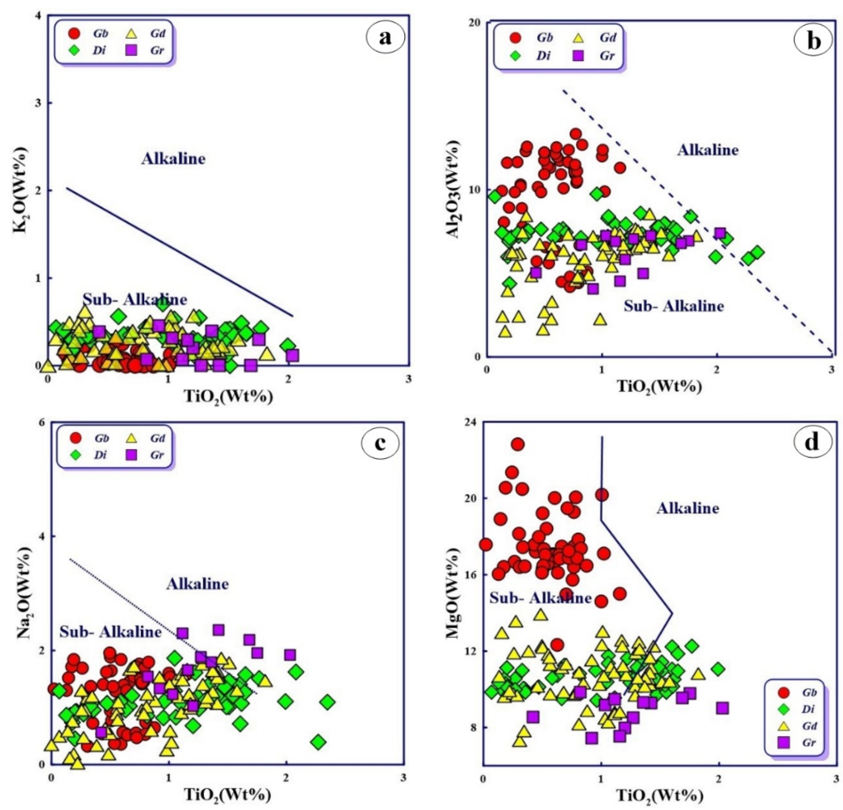

Figure14. Plots of amphibole compositions of the Gowd-e-Howz granitoid stock on the field of the subalkaline magmas of the subduction zones on the diagrams of TiO_2 vs. K_2O, Na_2O, Al_2O_3 and MgO (A-D) from [6].

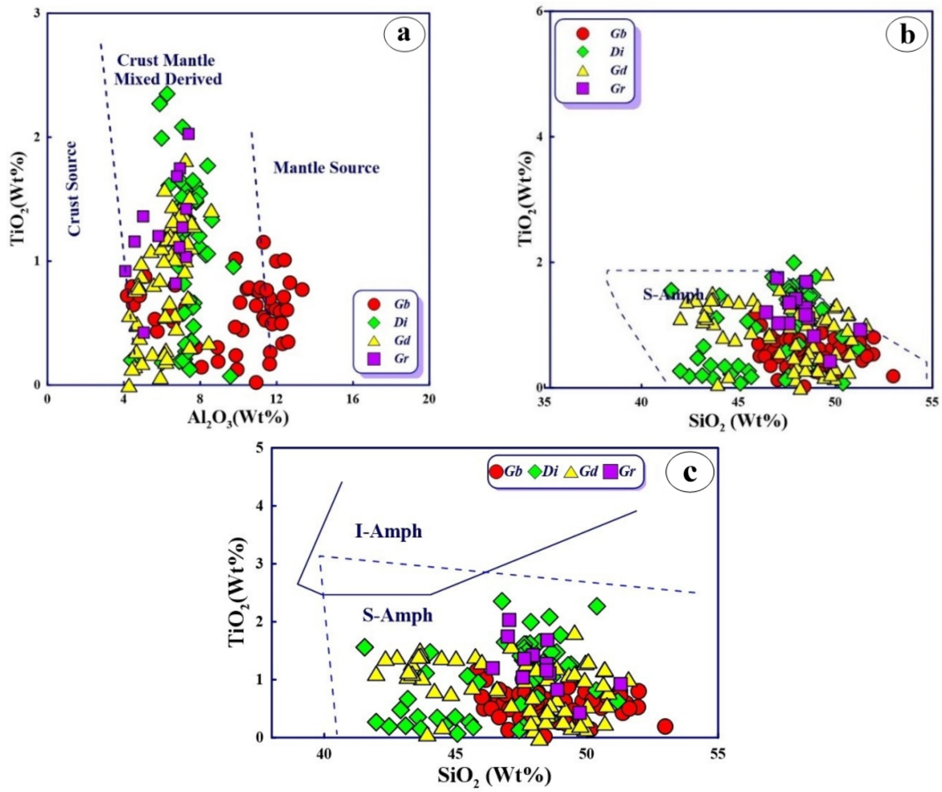

Figure15. Plots of amphibole compositions of the Gowd-e-Howz granitoid stock on the field of the subalkaline magmas of the subduction zones on the diagrams of A) TiO_2 vs. Al_2O_3 [3], B) SiO_2 vs. TiO_2 and C) SiO_2 vs. Na_2O [5-6].

Biotite chemistry depends largely upon the nature and composition of the parental magma. Biotites of the Gowd-e-Howz stock are medium titanium and iron rich pointing to a mixing process between mantle and crust magmas, confirmed also by Al_2O_3 vs. TiO_2 diagram [86] (Figure 7f). FeO, MgO, and Al_2O_3 contents in biotites can used for discriminating magma series and tectonic setting [4, 82]. The study biotites belong to the calc-alkaline series of the subduction zones (Figure 16) is consistent also with clinopyroxene (Figure 13) and amphibole chemistries (Figures 14, 15).

6.3. Mineralization Potential

Regarding the occurrence of mineralization potential of the Gowd-e-Howz granitoid stock, we investigated the fertility of this stock through chemical compositions of its biotite and plagioclase. Biotite as one of the most important ferromagnesian minerals of the granitoids also used to classify the genetic type of granitoids and their mineralization potential [4, 8, 54, 101-104]. Oxygen fugacity (fO_2) is a fundamental thermodynamic property governing redox potential in solid earth systems such as magma chambers of granitoids. During magma evolution, the fO_2 controls valence states of multivalent elements (e.g., Fe, Cu, Eu, Au, V, S, and C), which in turn controls their crystal/melt partitioning and solubility in silicate magmas. This is particularly crucial for ore mineralization in magmatic-hydrothermal systems and speciation of volatiles during magma degassing [8]. In the different mineral chemistry discriminating diagrams presented for distinguishing the granites into I, S, M, H, and A types, the Gowd-e-Howz granitoid rocks plot into the I-type granitoids. Lithological association (gabbro-diorite-granodiorite-granite), presence of MMEs, mineralogical features such as the dominant association of pyroxene, amphibole and plagioclase in mafic-intermediate rocks, the predominance of amphibole, brownish-green color biotite and plagioclase in felsic samples and the absence of metamorphic minerals such as muscovite, cordierite, garnet, corundum, andalusite, sillimanite and kyanite, along with the biotite chemical characteristics indicate the I-type magnetite series nature of the Gowd-e-Howz granitoid stock along with Cu mineralization potential (Figure 17).

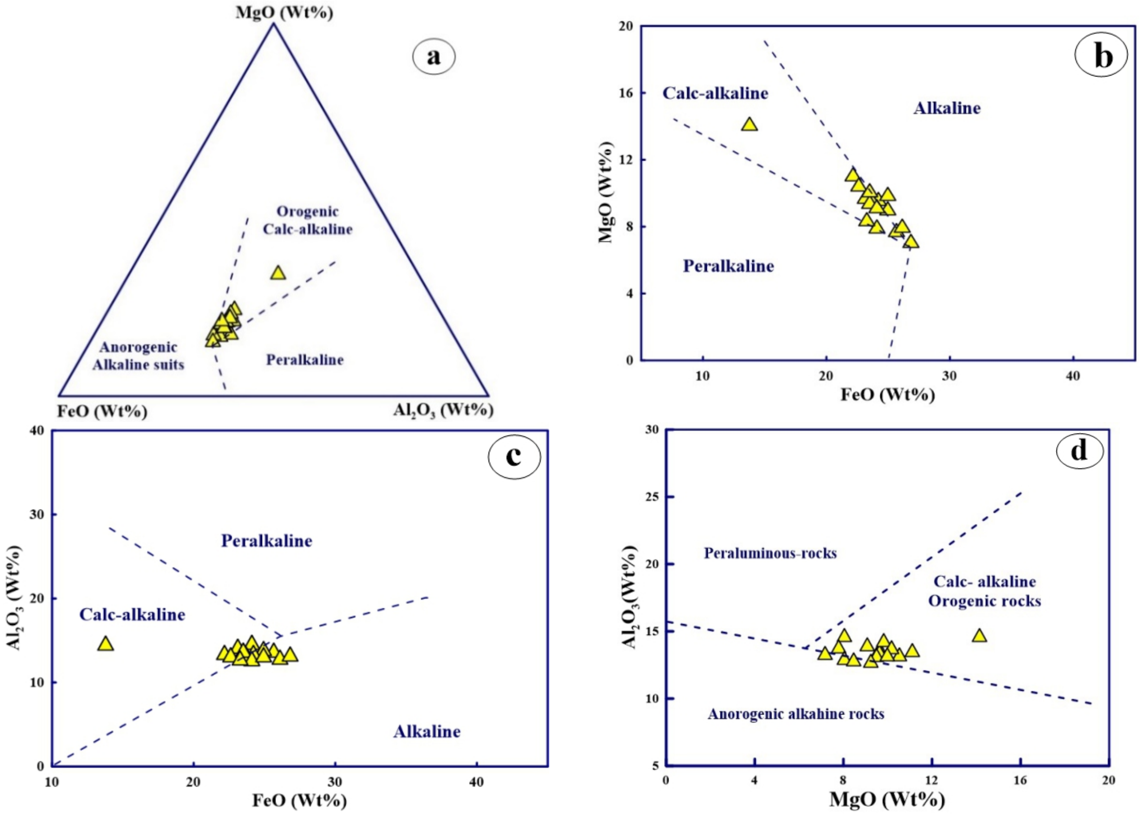

Figure16. Plots of biotite compositions of the Gowd-e-Howz granitoid stock on the field of the sub (calc)-alkaline orogenic magmas on the diagrams of: a) Al^{tot} vs. Mg from [82] and b) FeO vs. MgO, c) FeO vs. Al_2O_3, d) MgO vs. Al_2O_3 and e) MgO-FeO-Al_2O_3 from [4].

In the granitoids hosting the copper porphyry deposits, plagioclases from the mineralized intrusions might have higher alumina contents relative to the barren ones [107-111]. These authors argued that the low average of Al contents in plagioclase is most probably due to low P_{H2O} of melts. The ratio of Al/(Ca+Na+K) versus anorthite contents of plagioclase in the Gowd-e-Howz granitoid samples was used to discriminate mineralization potential of this stock. Compositions of the plagioclases mostly plot in the boundary line between the field of fertile and barren intrusions (Figure 18a), although, some samples plot in the fertile intrusion field and are in the range of the mineralized porphyry systems in the Urmia-Dokhtar magmatic belt (UDMB). The plagioclases that plot above 1:1 ratio line (Figure 18b) crystallized in an oxidized condition (close to the magnetite–hematite oxygen buffer) that is a common feature for Cu ± Mo porphyry systems [110-111]. The plagioclases of the Gowd-e-Howz granitoid samples mostly plot in the boundary line between the fields of oxidized and reduced intrusions (Figure 18b), although, some samples plot in the oxidized field.

6.4. Magma storage, crystallization and emplacement

The mineral data of clinopyroxene, amphibole and biotite offer three distinct sets of pressures and temperatures, which indicates three separate levels of major crystallization and thus magma chambers at ~45, ~15 and ~5-7 Km for storaging, differentiation and crystallization and final emplacement of magma into the continental crust (Figure 19b). Olivine, clinopyroxene and plagioclase are the early crystallized and the main minerals of mafic-intermediate part of the Gowd-e-Howz stock. The geothermobarometric calculations indicate that the clinopyroxenes crystallized at two levels (~ 45 and ~ 15 Km depths). Moreover, the Moho in the study region is at ~50 km depth [112-114]. Thus, it is assumed that earlier clinopyroxenes crystallized at T= ~1300°C and P= ~13 kbar, where the parent mafic magma emplaced in the base of the lower continental crust (Figure 19b).

Fractional crystallization of the dry minerals of olivine, clinopyroxene and plagioclase from parental mafic magma in the lower crust led to evolve magma from gabbro to diorite in composition. The diorite evolved magma was transported and storage into the middle crust (6.5-5 kbar =~15 Km depth) and crystallized clinopyroxene, amphibole, and plagioclase to form the main part of the stock as diorite-granodiorite. Finally, the more differentiated magma (granodiorite) migrated to the upper crust (3-1 kbar =~5 Km depth) to form the granitic part of the stock. The existence of calcic plagioclase phenocrysts and MMEs in the granodiorites provide evidence for magma recharge and subsequent magma mixing and mingling processes, while mineral compositional trends also suggest crystal fractionation. According to [115], arcs with young and thin crust are more probable to develop shallow magma reservoirs (e.g., 3-1 kbar below the surface) than arcs with old and thick crusts. The Upper Triassic magmatic arc of the SSMMZ as the first youngest thin arc of this zone was suitable candidate to emplacement of the Gowd-e-Howz stock (Figure 19a).

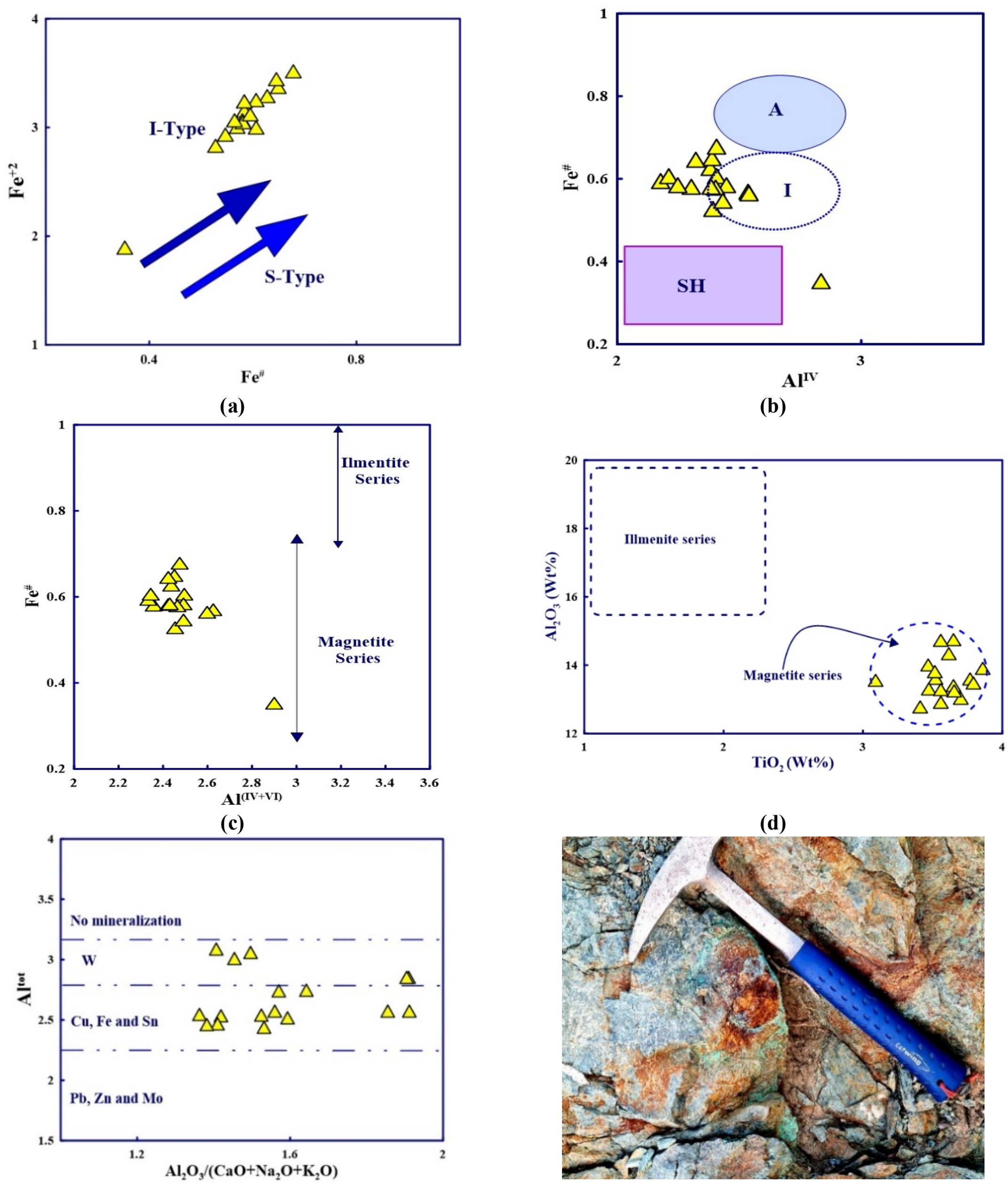

(e) (f)

Figure17. Plots of biotites compositions of the Gowd-e-Howz granitoid stock in the biotite chemistry-based different granite origin and mineralization potential determination diagrams. a) Binary Fe^{2+} vs. Fe^{3+} plot [105]. b) Binary Fe≠ vs. Al^{IV} plot [106]. c) Binary Fe≠ vs. Al^{IV+VI} plot [54]. d) Binary Al_2O_3 vs. TiO_2 plot [101]. e) Binary A/CNK of whole rock vs. Al^{tot} of biotite plot [97]. f) Existence of malachite mineral as an indicator of Cu minerallisation potential of Gowd-e-Howz granitoid body.

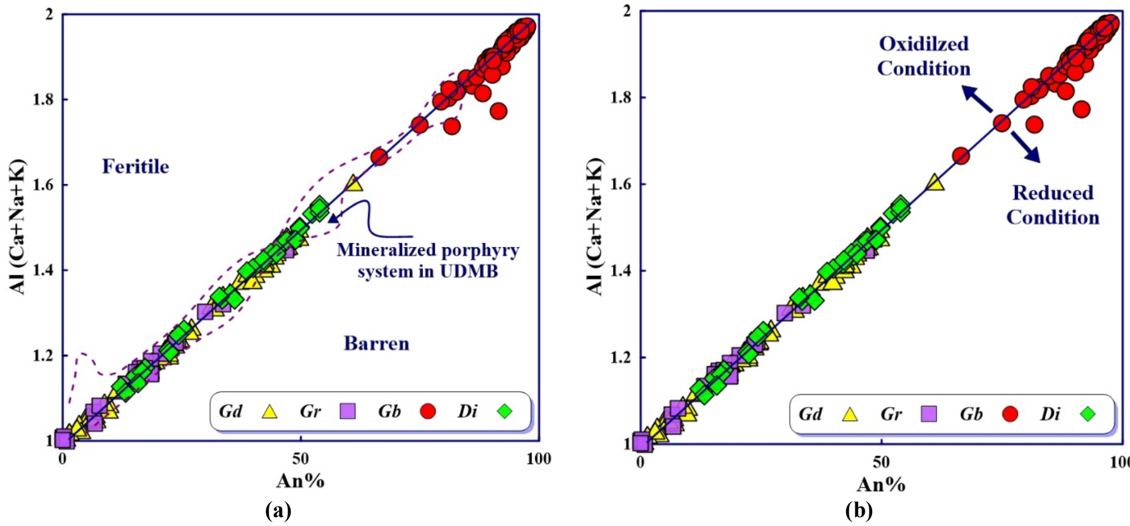

Figure18. Plots of plagioclase compositions of the Gowd-e-Howz granitoid stock in: a) The Al/(Ca+Na+K) vs. anorthite contents diagram [107, 110] for determining its mineralization potential. (b) The Al/(Ca+Na+K) vs. anorthite contents diagram to discriminate oxidized and reduced samples [110].

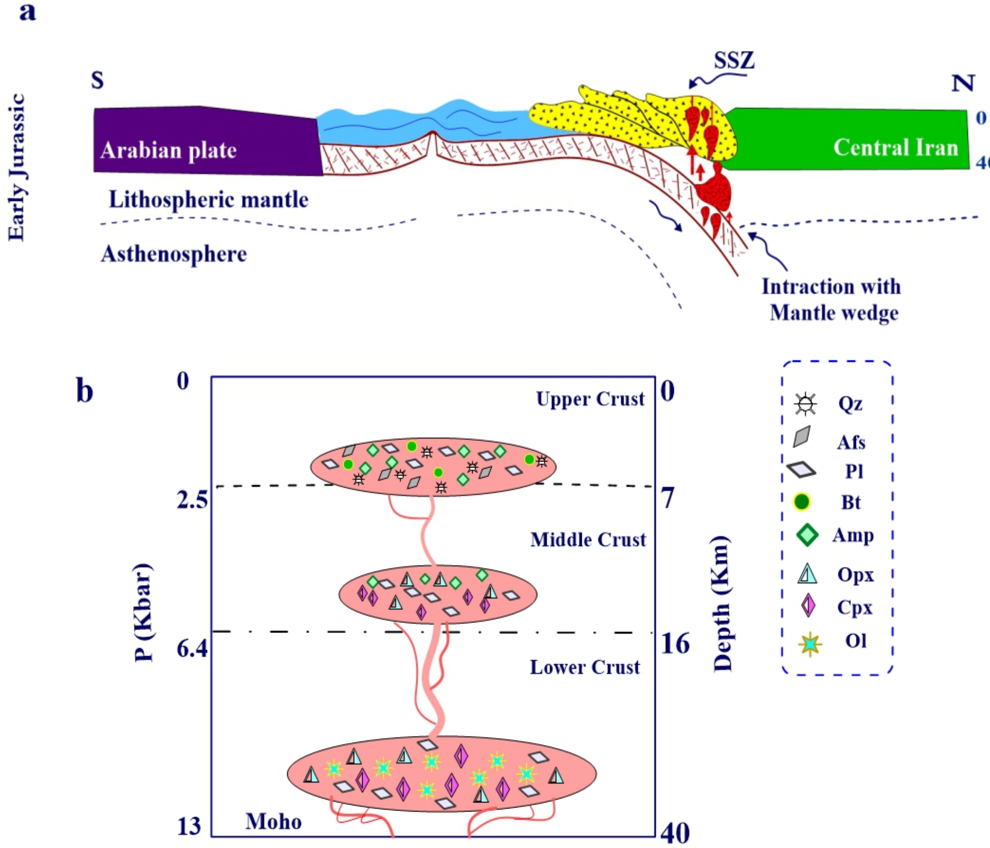

Figure19. Schematic geodynamic illustration of: a) How Early Jurassic subduction may cause and drawn in melts from subducting oceanic slab, mantle wedge and lower crust. b) How magma plumbing, storaging and fractionating occurred in three level in lower (40-50 Km), middle (14-16 Km) and upper (5-7 Km) crust.

6.5. Zircon U-Pb dates

One granodiorite (MH-1) and one granite (MH-21) samples from the Gowd-e-Howz granitoid stock selected for SHRIMP zircon U-Pb dating. Representative CL images of the analyzed zircon grains are presented in Figures 20b,d and U-Pb data are listed in Table 9. The zircon grains are euhedral to subhedral, mostly prismatic, and larger than 100 µm in length. They show oscillatory or sector zoning, indicative of a magmatic origin. In total, 24 points in MH-1 and 23 points in MH-21 have been dated. The U and Th contents of the zircon grains are 151–1561 and 48–1264 ppm, respectively, with Th/U ratios of 0.29–0.93 (Table 9), and no significant differences were observed between the samples. None of the grains has inherited cores with old age (Table 9). Zircon grains from the MH-1 and MH-21 granitoid samples yield weighted mean $^{206}Pb/^{238}U$ ages of 180 ± 1.5 Ma (N = 24; MSWD = 2.3) and 180 ± 1 Ma (N = 23; MSWD = 0.99), respectively (Figures 20a,c).

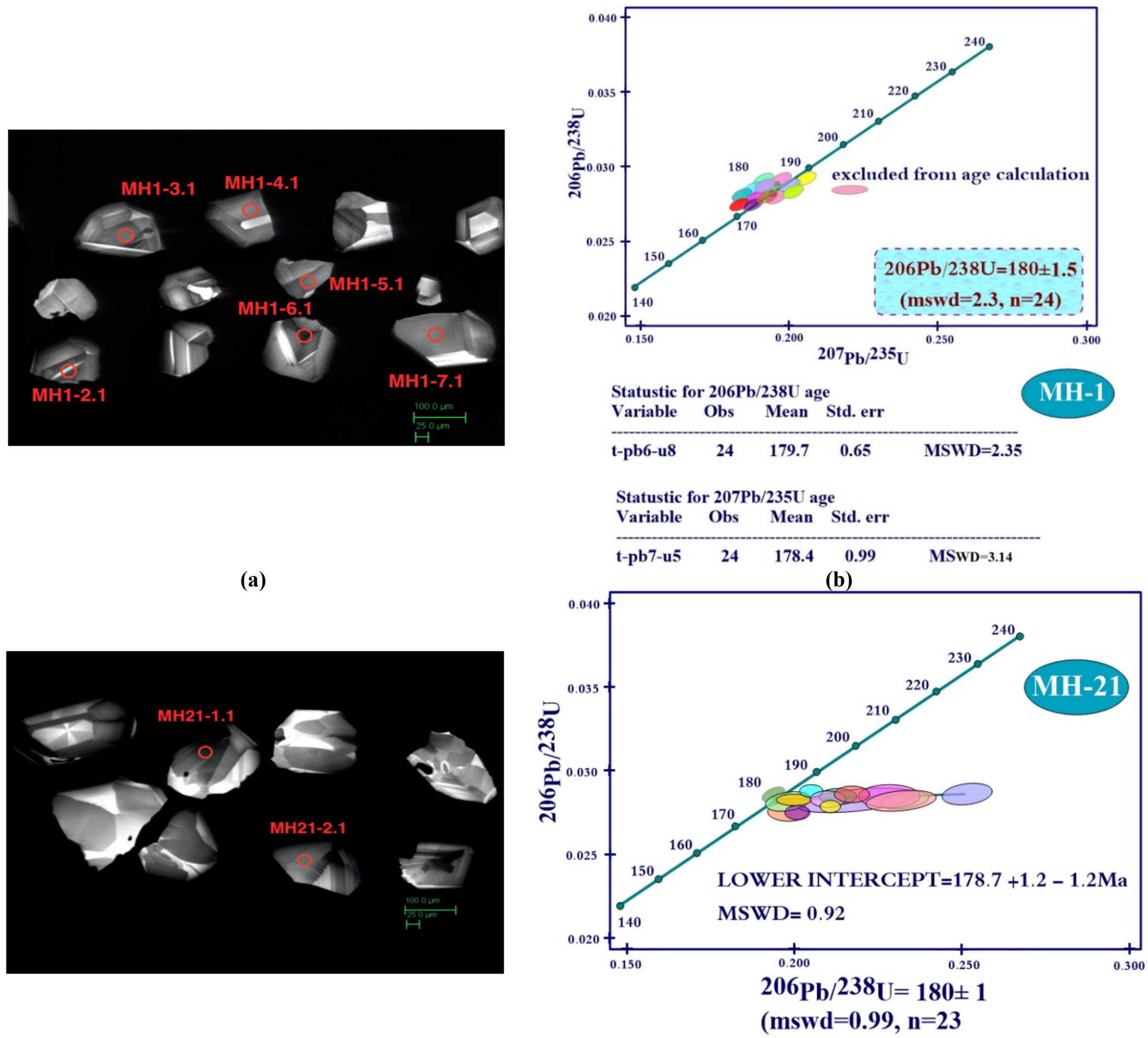

(c) (d)

Figure 20. a. Concordia diagram for analysed zircons of one granodiorite: 180 ± 1.5 Ma (MH-1) and b. its cathodoluminescence (CL) images of zircon grains. C. Concordia diagram for analysed zircons of one granite: 180 ± 1 Ma (MH-21) and d. its cathodoluminescence (CL) images of zircon grains.

6.6. Tectonic setting of the Gowd-e-Howz granitoid stock

The Late Carboniferous rifting event (~ 330 Ma) in the Iran plate related to the breakup of the Gondwana supercontinent and opened the Zagros Neotethyan Ocean between Iran and Arabia [15, 30]. Subsequently, during the Mesozoic-Cenozoic (since 220 Ma), Iran plate was formed through multiple accreted/subduction/collisional events [15]. The mineral compositions of the Lower Jurassic (180 ±1.5 Ma) Gowd-e-Howz granitoid stock represent that the rock types are I-type calc-alkaline nature, magnetite series that emplaced in a subduction environment. Based on the clinopyroxene, amphiboles and biotite source discrimination diagrams, it seem that the Gowd-e-Howz granitoid stock is the first magmatic product of subduction of Neotethyan Oceanic lithosphere beneath the central Iran plate (Figure 19a). These results are in good agreement with whole rock major, minor and trace element geochemistry discrimination diagrams [14].

7. Conclusions

According to the fieldworks and petrographic observations, the Lower Jurassic (180 ±1.5 Ma) Gowd-e-Howz granitoid stock from the SE Kerman, Iran, includes diorite, granodiorite and granite with minor amounts of gabbro. The stock intruded into the Upper Paleozoic-Triassic igneous and metamorphic rocks of the SSMMZ. Mineral chemistry of clinopyroxene show that they are medium to high-pressure calcic type with diopside-augite-salite composition, and belong to I-type calc-alkaline subduction zone magmatic series. Amphiboles are Mg-hornblende-tschermakite hornblende, ferro tschermakite, ferro tschermakite hornblende, ferro hornblende and tremolite hornblende. Some of amphiboles have tremolite-actinolite composition that probably formed by the retrograde replacement of pyroxenes. The biotites are of iron-bearing primary magmatic type. The mineral chemistry of clinopyroxene, amphibole and biotite indicate that the calc-alkaline (subalkaline) magma forming the Gowd-e-Howz granitoid stock produced in a young thin continental arc setting during the first phase of subduction of the Neotethyan oceanic lithosphere beneath the central Iran micro-plate in the Late Triassic-Early Jurassic times.

References

[1]. Le Bas, M.J. (1962). The Role of Aluminium in Igneous Clinopyroxenes with Relation to Their Parentage. *Am. J. Sci. 260(4):* 267-288.

[2]. Le Terrier, J., Maury, R. C., Thonon, P., Girard, D., & Marchal, M. (1982). Clinopyroxene composition as a method of identification of the magmatic affinities of paleo-volcanic series. *Earth and Plan. Sci. Lett. 59(1):* 139-154.

[3]. Jiang, C., & An, S. (1984). On the chemical characteristics of calcific amphiboles from igneous rocks and their petrogenesis significance. *J. Min. Petrol*. 3(1): 1-9.

[4]. Abdel-Rahman, A.M. (1994). Nature of biotites from alkaline, calc-alkaline, and peraluminous magmas. *J. Petrol.* 35 (2): 525-541. doi.org/10.1093/petrology/37.5.1025.

[5]. Coltorti, M., Bonadiman, C., Faccini, B., Grégoire, M., O'Reilly, S.Y., & Powell, W. (2007). Amphiboles from suprasubduction and intraplate lithospheric mantle. *Lithos* 99(1-2): 68-84. doi.org/10.1016/j.lithos.2007.05.009.

[6]. Molina, J.F., Scarrow, J.H., Montero, P.G., & Bea, F. (2009). High-Ti amphibole as a petrogenetic indicator of magma chemistry: Evidence for mildly alkali hybrid melts during evolution of Variscan basic–ultrabasic magmatism of Central Iberia. *Cont. Min. Petrol*. 158: 69-98. doi 10.1007/s00410-008-0371-4.

[7]. Putirka, K.D. (2016). Amphibole thermometers and barometers for igneous systems and some implications for eruption mechanisms of felsic magmas at arc volcanoes. *Am. Min.* 101(4): 841-858. doi.org/10.2138/am-2016-5506.

[8]. Li, W., Cheng, Y., & Yang, Z. (2019). Geo-fO2: Integrated software for analysis of magmatic oxygen fugacity. Geochem. *Geoph. Geosy*. 20. doi.org/10.1029/2019GC008273.

[9]. Lisboa, V.A.C., Conceição, H., Rosa, M.L.S., Marques, G.T., Lamarão, C.N., & Lima, A.L. (2020). Amphibole crystallization conditions as record of interaction between ultrapotassic enclaves and monzonitic magmas in the Glória Norte stock, south of Borborema province. *Braz. J. Petrol*. 50(2): 1-10. doi.org/10.1590/2317-4889202020190101.

[10]. Ridolfi, F. (2021). Amp-TB2: An Updated Model for Calcic Amphibole Thermobarometry. *Minerals* 11: 324. doi.org/10.3390/min11030324.

[11]. Wang, X., Hou, T., Wang, M., Zhang, Ch., Zhang, Zh., Pan, R., Marxer, F., & Zhang, H. (2021). A new clinopyroxene thermobarometer for mafic to intermediate magmatic systems. *Euro. J. Min.* 33: 621-637. doi.org/10.5194/ejm-33-621-2021.

[12]. Wieser, P. E., Kent, A. J. R., Till, C. B., Donovan, J., Neave, D. A., Blatter, D. L., & Krawczynski, M. J. (2023). Barometers Behaving Badly I: Assessing the Influence of Analytical and Experimental Uncertainty on Clinopyroxene Thermobarometry Calculations at Crustal Conditions. *J. Petrol.* 64: 1-27. doi.org/10.1093/petrology/egac126.

[13]. Sabzehei, M., Houshmandzadeh, A., Berberian, M., Nowgole Sadat, M.A.A., Alavi Tehrani, N., Majidi, B., Nazemzadeh, M., Azizan, H., & Roshan Ravan, J. (1993). Geological map of Haji Abad, Scale 1:250000. *Geological Survey of Iran, Tehran*.

[14]. Arvin, M., Pan, Y., Dargahi, S., Malekizadeh, A., & Babaei, A. (2007). Petrochemistry of the Siah-Kuh granitoid stock southwest of Kerman, Iran: Implications for initiation of Neotethys subduction. J. *Asian Earth Sci*. 30: 474-489. doi:10.1016/j.jseaes.2007.01.001.

[15]. Jafari, A., Ao, S., Jamei, S., & Ghasemi, H. (2023). Evolution of the Zagros sector of Neo-Tethys: Tectonic and magmatic events that shaped its rifting, seafloor spreading and subduction history. *Earth Sci. Rev*. 241, 104419. doi: 10.1016/j.earscirev.2023.104419.

[16]. Malekizadeh, A. (2000). Geochemistry and petrogenesis of the Siyah Kouh granite batholith. M.Sc. Thesis, *Shahid Bahonar University, Kerman, Iran.*

[17]. Ghanbarzadeh, N. (2011). Geochemistry, petrology and origin of the intermediate and asidic dykes in the Deh Sard area, SE Baft, Kerman. M.Sc. *Thesis, Shahid Bahonar University, Kerman, Iran.*

[18]. Alavi, M. (1994). Tectonics of Zagros Orogenic Belt of Iran, New Data and Interpretation. *Tectonophysics* 229: 211-238. doi.org/10.1016/0040-1951(94)90030-2.

[19]. Shabanian, N., & Neubauer, F. (2024). From Early Jurassic intracontinental subduction to Early-Middle Jurassic slab break-off magmatism during the Cimmerian orogeny in the Sanandaj-Sirjan Zone, Iran. *J. Asian Earth Sci.* 267: 106153. doi.org/10.1016/j.jseaes.2024.106153.

[20] Angiboust, S., Agard, Ph., Glodny, J., Omrani, J., & Oncken, O. (2016). Zagros blueschists: Episodic underplating and. long-lived cooling of a subduction zone. *Earth and Plan. Sci.* Let. 443: 48-58. http://dx.doi.org/10.1016/j.epsl.2016.03.017.

[21]. Azizi, H., Nouri, F., Stern, R.J., Azizi, M., Lucci, F., Asahara, Y., Zarinkoub, M.H., & Chung, S.L. (2018). New evidence for Jurassic continental rifting in the northern Sanandaj Sirjan Zone, western Iran: the Ghalaylan seamount, southwest Ghorveh. *INTER. GEOL. REV*. doi.org/10.1080/00206814.2018.1535913.

[22]. Barbero, E., Delavari, M., Dolati, A., Saccani, E., Marroni, M., Catanzariti, R., & Pandolfi, L. (2020). The Ganj Complex reinterpreted as a Late Cretaceous volcanic arc: Implications for the geodynamic evolution of the North Makran domain (southeast Iran). *J. Asian Earth Sci*. 195, 104306. doi.org/10.1016/j. jseaes.2020.104306.

[23]. Barbero, E., Pandolfi, L., Delavari, M., Dolati, A., Saccani, E., Catanzariti, R., Luciani, V., Chiari, M., & Marroni, M. (2021). The western Durkan Complex (Makran Accretionary Prism, SE Iran): a Late Cretaceous tectonically disrupted seamounts chain and its role in controlling deformation style. *Geosci. Front*. 12 (3), 101106.doi.org/ 10.1016/j.gsf.2020.12.001.

[24]. Gharibnejad, P., Rosenberg, C.L., Agard, P., Kananian, A., & Omrani, J. (2022). Structural and metamorphic evolution of the southern Sanandaj-Sirjan zone, southern Iran. *J. Earth Sc*i. https://doi.org/10.1007/s00531-022-02255-5.

[25]. Saccani, E., Delavari, M., Dolati, A., Pandolfi, L., Barbero, E. Tassinari, R., & Marroni, M. (2022). Geochemistry of basaltic blueschists from the Deyader Metamorphic Complex (Makran Accretionary Prism, SE Iran): New constraints for magma generation in the Makran sector of the Neo-Tethys. *J. Asian Earth Sci*. 228: 105141. doi.org/10.1016/j.jseaes.2022.105141.

[26]. Agard, P., Omrani, J., Jolivet, L., Whitechurch, H., Vrielynck, B., Spakman, W. Monié, P., Meyer, B. & Wortel, R. (2011). Zagros orogeny: a subduction-dominated process. *Geol. Mag*. 148(5-6): 692-725.

[27]. Hassanzadeh, J., & Wernicke, B.P. (2016). The Neotethyan Sanandaj-Sirjan zone of Iran as an arc type for passive margin-arc transitions. *Tectonics* 35(3): 586–621. doi:10.1002/2015TC003926.

[28]. Lechmann, A., Burg, J.P., Ulmer, P., Mohammadi, A., Guillong, M., & Faridi, M. (2018). From Jurassic rifting to Cretaceous subduction in NW Iranian Azerbaijan: geochronological and geochemical signals from granitoids. *Cont. Min. Petrol*. 173: 102. doi.org/10.1007/s00410-018-1532-8.

[29]. Azizi, H., & Whattam, S.A. (2022). Does Neoproterozoic-Early Paleozoic (570–530 Ma) basement of Iran belong to the Cadomian Orogeny? Precam. Res. 368 (2022) 106474. https://doi.org/10.1016/*j.precamres.2021*.106474.

[30]. Asadi, S.A.A., Ghasemi, H., Sepidbar, F., Mobasheri, M., Shi, Y., & Palin, R. M. (2023). A polygenetic origin for the Sikhoran ultramafic-mafic complex in South Iran. *Lithos* 456-457. 107336. doi.org/10.1016/j.lithos.2023.107336.

[31]. Mehdipour Ghazi, J. & Moazzen, M. (2015). Geodynamic evolution of the Sanandaj-Sirjan Zone, Zagros Orogen, Iran. *Turk. J. Earth Sci. 24: 513-528.* doi:10.3906/yer-1404-12.

[32]. Hassanzadeh, J., Stockli, D.F., Horton, B.K., Axen, G.J., Stockli, L.D., Grove, M., Schmitt, A.K. & Walker, J.D. (2008). U-Pb zircon geochronology of late Neoproterozoic- Early Cambrian granitoids in Iran. Implications for paleogeography, magmatism, and exhumation history of Iranian basement. *Tectonophysics 451*: 71-96.

[33]. Moghadam, H. S., Brocker, M., Griffin, W. L., Li, X. H Chen, R. X., & O'Reilly1 S. Y. (2017). Subduction, high–P metamorphism and collision fingerprints in SW Iran: Constraints from zircon U-Pb and mica Rb–Sr geochronology. *Geochem. Geoph. Geosy. 18*: 306-332. doi: 10.1002/2016GC006585.

[34]. Ghasemi, H., Juteau, T., Bellon, H., Sabzehei, M., Whitechurch, H., & Ricou, L.E. (2002). The mafic-ultramafic complex of Sikhoran (Central Iran): A polygenetic ophiolite complex. *C. R. Geosci.* 334: 431-438. doi.org/10.1016/S1631-0713(02)01770-4.

[35]. Ghasemi, H., Sabzehei, M., Juteau, T., Bellon, H., & Emami, M.H. (2004). Radiometric age of mafic parts and metamorphic hosts of Sikhoran ultramafic-mafic complex, southeastern Iran. *Geosci.* 11(51-52): 58-67 (in Persian).

[36]. Ahmadipour, H., Sabzehei, M., Emami, M., Whitechurch, H., & Rastad, E. (2003). Soghan complex as an evidence for paleo spreading center and mantle diapirism in Sanandaj-Sirjan zone (south-east Iran*). J. Sci. Islam. Repub. Iran 14*: 157-172.

[37]. Baharifar, A., Moinevaziri, H., Bellon, H. & Piqué, A. (2004). The crystalline complexes of Hamadan (Sanandaj – Sirjan zone, western Iran): Meta-

sedimentary Mesozoic sequences affected by Late Cretaceous tectono-metamorphic and plutonic events. *C. R. Geosci. 336*: 1443-1452.

[38]. Fazlnia, A., Schenk, V., Appel, P., & Alizade, A. (2013). Petrology, geochemistry, and geochronology of the Chah-Bazargan gabbroic intrusions in the south Sanandaj-Sirjan zone, Neyriz, Iran. Inter. *J. Earth Sci. 102*: 1403-1426, doi:10.1007/s00531-013-0884-6.

[39]. Didier, J., & Barbarin, B. (1991). The different types of enclaves in granites-nomenclature. In: J. Didier, & Barbarin, B. (Eds.). *Enclaves and granite petrology: Development in Petrology. Elsevier, Amsterdam*: 19-24. http://pascal-francis.inist.fr/vibad/index.php?action= getRec ordDetail&idt= 6546938.

[40]. Vernon, R. H. (1984). Microgranitoid enclaves in granites - globules of hybrid magma quenched in a plutonic environment. Nature 309: 438-439. doi.org/10.1038/309438a0.

[41]. Vernon, R.H. (2004). A practical guide to rock microstructures. *Cambridge University Press*. 594p.

[42]. Morimoto, N., Fabrise, J., Ferguson, A., Ginzburg, I. V., Ross, M., Seifert, F.A., Zussman, J., Akoi, K., & Gottardi, G. (1988). Nomenclature of pyroxenes. *Am. Min. 173*: 1123-1133.

[43]. Leake, B.E., Woolley, A.R., Arps, C.E., Birch, W.D., Gilbert, M.C., Grice, J.D., Hawthorne, F.C., Kato, A., Kisch, H.J., & Krivovichev, V.G. (1997). Nomenclature of amphiboles; report of the Subcommittee on Amphiboles of the International Mineralogical Association Commission on new minerals and mineral names. *Min. mag. 61(405)*: 295-310.

[44]. Yavuz, F., & Döner, Z. (2017). WinAmptb: A Windows program for calcic amphibole thermobarometry. *Periodico di Min. 86*: 135-167. doi: 10.2451/2017PM710.

[45]. Putirka, K.D. (2008). Thermometers and barometers for volcanic systems. *Rev. Min. Geochem. 69(1)*: 61-120. doi.org/10.2138/rmg.2008.69.3.

[46]. Nimis, P., & Taylor, W. (2000). Single clinopyroxene thermobarometry for garnet peridotites. Part I. Calibration and testing of a Cr-in-Cpx barometer and an enstatite-in-Cpx thermometer. *Cont. Min. Petrol. 139*: 541-554. doi.org/10.1007/s004100000156.

[47]. Williams, I. S., & Claesson, S. (1987). Isotopic evidence for the Precambrian provenance and Caledonian metamorphism of high grade paragneisses from the Seve Nappes, Scandinavian Caledonides. II: Ion microprobe zircon U-Th-Pb. *Cont. Min. Petrol. 97*: 205-217.

[48]. Claoue-Long, J. C., Compston, W., Roberts, J., & Fanning, C. M. (1995). Two Carboniferous ages: a comparison of SHRIMP zircon dating with conventional zircon ages and 40Ar/39Ar analysis. In: Berggren, W. A., Kent, D. V., Aubry, M. P., & Hardenbol, J. (Eds.). Geochronology Time Scales and Global Stratigraphic Correlation. *SEPM (Society for Sedimentary Geology) Special Publication No.* 4: 3-21.

[49]. Black, L. P., Kamo, S. L., Allen, C. M., Aleinikoff, J. A., Davis, D. W., Korsch, J. R., & Foudolis, C. (2003). TEMORA 1: a new zircon standard for Phanerozoic U-Pb geochronology. *Chem. Geol. 200*: 155-170.

[50]. Nisbet, E. G., & Pearce, J. A. (1977). Clinopyroxene composition in mafic lavas from different tectonic Settings. *Cont. Min. Petrol. 63*: 149-160.

[51]. Anderson, J.L. (1996). Status of thermobarometry in granitic batholiths, Earth and Env. Sci. Trans. *Royal Society of Edinburgh. 87(1-2)*: 125-138. doi: 10.1017/S0263593300006544.

[52]. Anderson, J.L. 1997. Status of thermobarometry in granitic batholiths. Earth and Env. Sci. Trans. *The Royal Society of Edinburgh. 87*: 125-138. http://journals.cambridge.org/abstract-S0263593300006544.

[53]. Anderson, J.L., & Smith, D.R. (1995). The effect of temperature and oxygen fugacity on Al-in-hornblende barometry. *Am. Min. 80(5-6)*: 549-559.

[54]. Anderson, J.L., Barth, A.P., Wooden, J.L., Mazdab, F., 2008. Thermometers and thermobarometers in granitic systems*. Rev. Min. Geochem. 69*: 121-142. https://doi.org/10.2138/rmg.2008.69.4.

[55]. Andrews, B.J., Gardner, J.E., & Housh, T.B. (2008). Repeated recharge ,assimilation, and hybridization in magmas erupted from El Chichón as recorded by plagioclase and amphibole phenocrysts. *J. Volcan. Geoth. Res. 175(4)*: 415-426.

[56]. Blundy, J.D. & Holland, T.J.B. (1990). Calcic amphibole equilibria and a new amphibole-plagioclase geothermometer. *Cont. Min. Petrol. 104*: 208-24.

[57]. Ernst, W., & Liu, J. (1998). Experimental phase-equilibrium study of Al-and Ti-contents of calcic amphibole in MORB-A semiquantitative thermobarometer. *Am. Min. 83*: 952-969. doi.org/10.2138/am-1998-9-1004.

[58]. F´em´enias, O., Mercier, J.C.C., Nkono, C., Diot, H., Berza, T., Tatu, M., & Demaiffe, D. (2006). Calcic amphibole growth and compositions in calc-alkaline magmas: Evidence from the Motru dike swarm (southern Carpathians, Romania*). Am. Min. 91*: 73-81. doi: 10.2138/am.2006.1869.

[59]. Hammarstrom, J.M., & Zen, E.-a. (1986). Aluminum in hornblende: an empirical igneous geobarometer. *Am. Min. 71(11-12)*: 1297-1313.

[60]. Helmy, H., Ahmed, A., El Mahallawi, M., & Ali, S. (2004). Pressure, temperature and oxygen fugacity conditions of calc-alkaline granitoids, Eastern Desert of Egypt, and tectonic implications. J. Afr. *Earth Sci. 38(3)*: 255- 268.

[61]. Johnson, M.C., & Rutherford, M.J. (1989). Experimental calibration of an aluminum-in-hornblende geobarometer with application to Long Valley caldera (California) volcanic rocks. *Geology 17(9)*: 837-841.

[62]. Kretz, R. (1994). Metamorphic Crystallization. *John Wiley & Sons. New York*. 507p.

[63]. Lindsley, D. H. (1983). Pyroxene thermometry. *Am. Min. 68*: 477-493.

[64]. Luhr, J.F., Carmichael, I.S. & Varekamp, J.C. (1984). The 1982 eruptions of El Chichón Volcano, Chiapas, Mexico: mineralogy and petrology of the anhydrite bearing pumices. *J. Volcan. Geoth. Res. 23(1-2)*: 69-108. 10.1016/0377-0273(84)90057-X.

[65]. Ridolfi, F., Renzulli, A., & Puerini, M. (2010). Stability and chemical equilibrium of amphibole in calc-alkaline magmas: An overview, new thermobarometric formulations and application to subduction-related volcanoes. *Cont. Min. Petrol. 160(1)*: 45-66. doi 10.1007/s00410-009-0465-7.

[66.] Ridolfi, F., & Renzulli, A. (2012). Calcic amphiboles in calc-alkaline and alkaline magmas: Thermobarometric and chemometric empirical equations valid up to 1,130° C and 2.2 GPa. *Cont. Min. Petrol. 163(5)*: 877-895. doi 10.1007/s00410-011-0704-6.

[67]. Ridolfi, F., Renzulli, A., Perugini, D., Cesare, B., Braga, R., & Del Moro, S. (2016). Unravelling the complex interaction between mantle and crustal magmas encoded in the lavas of San Vincenzo (Tuscany, Italy). Part II: Geochemical overview and modelling. *Lithos* 244: 233-249. doi:10.1016/j.lithos.2015.09.029.

[68]. Scaillet, B., & Evans, B.W. (1999). The 15 June 1991 eruption of Mount Pinatubo. I. Phase equilibria and pre-eruption P-T-f O2-f H2O conditions of the dacite magma. *J. Petrol. 40(3)*: 381-411. doi: 10.1093/petroj/40.3.381.

[69]. Schmidt, M.W. (1992). Amphibole composition in tonalite as a function of pressure: An experimental calibration of the Al-in-hornblende barometer. *Cont. Min. Petrol. 110*: 304-310.

[70]. Schweitzer, E. L., Papike, J. J. & Bence, A. E. (1979). Statistical analysis of clinopyroxenes from deep-sea basalts. *Am. Min. 64*: 501-513.

[71]. Soesoo, A. (1997). A multivariate statistical analysis of clinopyroxene composition: Empirical coordinates for the crystallisation PT-estimation. *Geol. Soci. Swed. (Geologiska Föreningen) 119*: 55-60.

[72]. Stein, E., & Dietl, C. (2001). Hornblende thermobarometry of granitoids from the Central Odenwald (Germany) and their implications for the geotectonic development of the Odenwald. *Min. petrol. 72 (1)*: 207-285. www.researchgate.net/publication/225775322.

[73]. Sial, A., Ferreira, V., Fallick, A., & Cruz, M.J.M. (1998). Amphibole-rich clots in calc-alkali granitoids in the Borborema province, northeastern Brazil. *J. South Am. Earth Sci. 11(5)*: 457-471.

[74]. Hawthorne, F.C., Oberti, R., Harlow, G.E., Maresch, W.V., Martin, R.F., Schumacher, J.C., & Welch, M.D. (2012). Nomenclature of the amphibole super group. *Am. Min. 97(11-12)*: 2031-2048. doi.org/10.2138/am.2012.4276

[75]. Giret, A., Bonin, B., & Leger, J.M., 1980. Amphibole compositional trends in oversaturated and undersaturated alkaline plutonic ring-complexes. *Can. Min. 18*, 481/495.

[76]. Hawthorne, F.C., & Oberti, R. (2007). Classification of the Amphiboles. *Rev. Min. Geochem. 67*: 55-88. doi: 10.2138/rmg.2007.67.2.

[77] .Deer, W.A., Howie, R.A., & Sussman, J. (1991). An introduction to the rock forming minerals. *Longman Ltd*. 528p. www.geokniga.org/bookfiles/geokniga-anintroductiontotherock-formingminerals.pdf.

[78]. Partin, E., Hewitt, D.A., & Wones, D.R. (1983). Quantification of ferric iron in biotite, *Geol. Soci. Am. Abstract with programs 15*: 659.

[79]. Wones, D.R., Burns, R.G., & Carrol, B.M. (1971). Stability and properties of synthetic annite. *Am. Geophy. Uni. Trans. 52*: 369.

[80]. Abbot R.N. Jr., & Clarke, D.B. (1979). Hypothetical liquidus relationships in the subsystem Al2O3-FeO-MgO projected from quartz, alkali feldspar and plagioclase for (H2O) < 1. *Can. Min. 17*: 549-560.

[81]. Henry, D.J., Guidotti, C.V., & Thomson, J.A. (2005). The Ti-saturation surface for low-to-medium pressure metapelitic biotite: Implications for Geothermometry and Ti-substitution Mechanisms. *Am. Min. 90(2-3)*: 316-328. doi.org/10.2138/am.2005.1498.

[82]. Nachit, H., Razafimahefa, N., Stussi, J.M & Caron, J.P. (1985). Composition chimique des biotites et typologie magmatique des granitoïdes. *C. R. Acad. Sci. Paris, Ser. II 301*: 813-818.

[83]. Nachit, H., Ibhi, A., Abia, El.-H. & Ohoud, M.B. (2005). Discrimination between primary magmatic biotites, reequilibrated biotites and neoformed biotites. *C. R. Geosci. 337(16):* 1415-1420. doi.org/10.1016/j.crte.2005.09.002.

[84]. Abrecht, J. & Hewitt, D.A. (1988). Experimental evidence on the substitution of Ti in biotite. *Am. Min. 73(11-12)*: 1275- 1284. www.minsocam.org/ammin/AM73/AM7 3-1275.pdf.

[85]. Foster, M.D. (1960). Interpretation of the composition of trioctahedral micas. *U.S. Geological Survey Professional Paper, Washington*, 49 pp. pubs.usgs.gov/pp/0354b/report.

[86]. Zhao, K., Jiang, S., Yang, S., Daí, B., & Lu, J. (2012). Mineral chemistry, trace elements and Sr-Nd-Hf

isotope geochemistry and petrogenesis of Cailing and Furong granites and mafic enclaves from the Qitianling batholith in the Shi-Hang zone, South China. *Gondw. Res. 22*: 310-324. doi.org/10.1016/j.gr.2011.09.010.

[87]. Nimis, P.A. (1995). Clinopyroxene geobarometer for basaltic systems based on crystal-structure modeling. *Cont. Min. Petrol. 121*: 115-125. doi.org/10.1007/s004100050093.

[88]. Wood, B. J., & Banno, S. (1973). Garnet-Orthopyroxene and orthopyroxene-clinopyroxene relationships in simple and complex systems. *Cont. Min. and Petrol. 42*: 109-124.

[89]. Wells, P. R. A. (1977). Pyroxene thermometry in simple and complex systems. *Cont. Min. Petrol. 62*: 129-139.

[90]. Davidson, P. M. (1985). Thermodynamic analysis of quadrilateral pyroxenes. Part 1: Derivation of the ternary nonconvergent site-disorder model. *Cont. Min. Petrol. 91*: 383-389.

[91]. Davidson, P. M., & Lindsley, D. H. (1985). Thermodynamic analysis of quadrilateral pyroxenes. Part 2: model calibration from experiments and application to geothermometry. *Cont. Min. Petrol. 91*: 390-404.

[92]. Yavuz, F. (2013). WinPyrox: A Windows program for pyroxene calculation classification and thermobarometry. *Am. Min. 98*: 1338-1359. doi.org/10.2138/am.2013.4292.

[93]. Bertrand, P., & Mercier, J. C. (1985). The mutual solubility of coexisting ortho and clinopyroxene: Toward an absolute geothermometr for natural systems? Earth and Plan. *Sci. Lett. 76*: 109-122.

[94]. Elkins, L.T., & Grove, T.L. (1990). Ternary feldspar experiments and thermodynamic models. *Am. Min. 75*:544-559.

[95]. Hollister, L.S., Grissom, G., Peters, E., Stowell, H., & Sisson, V. (1987). Confirmation of the empirical correlation of Al in hornblende with pressure of solidification of calc-alkaline plutons. *Am. Min. 72(3-4)*: 231-239.

[96]. Patino Douce, A. (1993). Titanium substitution in biotite: an empirical model with applications to thermometry, O2 and H2O barometries, and consequences for biotite stability. *Chem. Geol. 108(1–4)*: 133-162. doi.org/10.1016/0009-2541(93)90321-9.

[97]. Uchida, E., Endo, S. & Makino, M. (2007). Relationship between solidification depth of granitic rocks and formation of hydrothermal ore deposits. *Reso. Geol. 57(1)*: 47-56. doi.org/10.1111/j.1751-3928.2006.00004.x.

[98]. Avanzinelli, R., Bindi, L., Menchetti, S., & Conticelli, S. (2004). Crystallisation and genesis of peralkaline magmas from Pantelleria Volcano, Italy: an integrated petrological and crystal-chemical study. *Lithos 73*: 41-69. doi: 10.1016/j.lithos.2003.10.007.

[99]. Zhu, Y., & Ogasawara, Y. (2004). Clinopyroxene phenocrysts (with green salite cores) in trachybasalts: implications for two magma chambers under the Kokchetav UHP massif, North Kazakhstan. *J. Asian Earth Sci. 22(5)*: 517-527. doi.org/10.1016/S1367-9120(03)000919.

[100] .Molina, J.F., Moreno, J.A., Castro, A., Rodríguez, C., & Fershtater, G.B. (2015). Calcic amphibole thermobarometry in metamorphic and igneous rocks: New calibrations based on plagioclase/amphibole Al-Si partitioning and amphibole/liquid Mg partitioning. *Lithos, 232*, 286-305. doi.org/10.1016/j.lithos.2015.06.027.

[101]. Karimpour, M.H., Stern, C.R., Mouradi, M., (2011). "Chemical composition of biotite as a guide to petrogenesis of granitic rocks from Maherabad, Dehnow, Gheshlagh, Khajehmourad and Najmabad, Iran". *Journal of Crystallography and Mineralogy, 18(4)*, 89-100. ijcm.ir/article-1-502-en.html.

[102]. Azadbakht, Z., Lentz, D.R., McFarlane, C.R.M., Whalen, J.B., (2020). "Using magmatic biotite chemistry to differentiate barren and mineralized Silurian- Devonian granitoids of New Brunswick, Canada". *Contribution to Mineralogy and Petrology,* 175. doi.org/10.1007/s00410- 020-01703-2.

[103]. Khosravi, M., Christiansen, E.H., Rajabzadeh, M.A., (2021). "Chemistry of rockforming silicate and sulfide minerals in the granitoids and volcanic rocks of the Zefreh porphyry Cu-Mo deposit, central Iran: implications for crystallization, alteration, and mineralization potential. *Ore Geology Review*". doi.org/10.1016/j.oregeorev.2021.104150.

[104]. Kumar, A.A., Ashok, Ch., (2023). "Geochemistry and mineral chemistry of the armoor granitoids, eastern dharwar craton: implications for the redox conditions and tectonomagmatic environment". *Acta Geochim.* doi.org/10.1007/s11631-023-00647-1.

[105]. Villaseca, C., Ruiz-Martı´nez, V.C., Pe´rez-Soba, C., (2017). "Magnetic susceptibility of Variscan granite-types of the Spanish central system and the redox state of magma". *Geol Acta, 15*, 379-394. doi.org/10.1344/GeologicaActa2017.15.4.8

[106]. Jiang, Y.H., Jiang, S.Y., Ling, H.F., Zhou, X.R., Rui, X.J. and Yang, W.Z., (2002). "Petrology and geochemistry of shoshonitic plutons from the western Kunlun orogenic belt, Xinjiang, northwestern China: implications for granitoid geneses". *Lithos, 63(3-4),* 165-187. 10.1016/ S0024- 4937(02) 00140-8.

[107]. Williamson, B.J., Herrington, R. J., & Morris, A. (2016). Porphyry copper enrichment linked to excess aluminium in plagioclase. *Nature Geosci. 9*: 237-241.

[108]. Richards, J.P. (2016). Clues to hidden copper deposits. *Nature Geosci. 9*: 195-196.

[109]. Zarasvandi, A., Rezaei, M., Raith, J.G., Pourkaseb, H., Asadi, S., Saed, M., & Lentz, D. R. (2018). Metal endowment reflected in chemical composition of silicates and sulfides of mineralized porphyry copper systems, Urumieh-Dokhtar magmatic arc, Iran. *Geoch. Cosm. Acta, 223*: 36-59.

[110]. Rezaei, M., & Zarasvandi, A. (2022). Combined Feldspar-Destructive Processes and Hypogene Sulfide Mineralization in the Porphyry Copper Systems: Potentials for Geochemical Signals of Ore Discovering. Ir. *J. Sci. and Tech. 46*: 1413-1424.

[111]. Sepahi, A.A., Nemati, B., Asiabanha, A., Miri, M., & Deniz, K. (2023). Mineral chemistry and petrology of magmatic rocks from NW Takestan (NW Iran). *Geopersia 13(1)*: 123-143 doi: 10.22059/GEOPE.2023.350569.648686.

[112]. Dehghani, G.A., & Makris, J. (1984). The gravity field and crustal structure of Iran. *N. Jb. Geol. Palaontol. Agh. 168*:215-229.

[113]. Tatar, M., & Nasrabadi, A. (2013). Crustal thickness variations in the Zagros continental collision zone (Iran) from joint inversion of receiver functions and surface wave dispersion. *J. Seismo*. doi 10.1007/s10950-013-9394-z.

[114]. Motaghi, K., Shabanian, E. & Kalvandi, F. (2017). Underplating along the northern portion of the Zagros suture zone, Iran. *Geophy. J. Inter. 210(1)*: 375-389. doi.org/10.1093/gji/ggx168.

[115]. Chaussard, E. & Amelung, F. (2014). Regional controls on magma ascent and storage in volcanic Arcs. *Geochem. Geoph. Geosy.* 1407-1418.

[116]. Humphreys, MC.S, Blundy, J.D, & Sparks, R.S.J. (2006). Magma evolution and open-system processes at Shiveluch volcano: Insights from phenocryst zoning. *J. Petrol. 47*: 2303-2334. doi:10.1093/petrology/egl045.

Appendix

A. Thermometry by [58] method

A quantitative thermometer applicable to high-T (>700 °C) amphibole crystalizing in Ti-saturated calc-alkaline magmas proposed by [58]. Their T estimates are globally in agreement with those deduced from the [56] thermometer. Solubility of Ti in calcic amphibole buffered by a Ti-rich phase displays an ideal solid-solution behavior. Their thermometry equation with uncertainty ranges from ±15 to ±55 °C is as follows:

$$\ln[Ti]_{Amphibole} = 2603/T - 1.70 \quad (10)$$

Where [Ti] amphibole expressed in atoms per formula unit (apfu). Applying this equation to the amphibole-plagioclase data from the Gowd-e-Howz granitoid stock gave the temperatures range of 569-771°C (Table 9) for the final replacement of the stock and the stop of the cations exchange and final equilibrium of the amphibole-plagioclase pairs.

B. Thermometry by [115] method

Following equation with an uncertainty range of ±35 to ±45 [115], proposed to obtain the temperature of amphibole crystallization as follows:

$$T = 479.8(Na + K)_{[A]} + 643.5 \quad (11)$$

Applying this method to the amphiboles of the Gowd-e-Howz granitoid stock gave the temperatures range of 646-871°C (Table 9) for the final replacement of the stock and the stop of the cations exchange and final equilibrium of the amphibole-plagioclase pairs.

C. Thermometry by [7] method

Following equation as an amphibole geothermometer presented by [7]:

$$T[°C]=1781-132.74\times Si_{Amph}+116.6\times Ti_{Amph} -69.41\times Fet_{Amph}+101.62\times Na_{Amph} \quad (12)$$

Applying this method to the amphiboles of the rocks of the Gowd-e-Howz granitoid stock represents the temperatures in Table 9 for the final replacement of the stock and the cessation of the exchange and the final equilibrium of the amphibole-plagioclase pairs.

D. Thermometry by [67] method

Geothermometer equation for determining the amphibole temperature is as follow:

$$T=25.3\times P+645.9 \quad (13)$$

Temperatures obtained by this method for amphiboles of the Gowd-e-Howz granitoid stock range between 667 to 678°C (Table 9), which are low to amphibole crystallization temperature and are the closing T for final replacement of the stock and stopping of the cations exchange and final equilibrium of the amphibole-plagioclase pairs.

A graphical thermometric based on amounts of Al^{IV} versus Ti in amphiboles presented by [57] (Figure 13-a). The amphiboles of the Gowd-e-Howz granitoid stock plot in temperature ranges of 650 to 900°C in this graph. Naturally, the higher temperatures are close to the crystallization temperatures and the lower ones correspond to the closing temperatures. The diagram of Ti versus (Na+K) from [68] also used as an amphibole thermometer for the Gowd-e-Howz granitoid stock, that shows the T in ranges lower than 750 °C (Figure 13-b).

انجمن مهندسی معدن ایران
نشریه مهندسی معدن و محیط زیست
نشانی نشریه: www.jme.shahroodut.ac.ir
دانشگاه صنعتی شاهرود

شیمی کانی استوک گرانیتوئیدی گودحوض، جنوب خاوری ایران: پتانسیل کانی‌زایی در رابطه با جایگاه تکتونوماگمایی

محبوبه عرب‌زاده بنی‌اسدی، حبیب اله قاسمی[1*]، مهدی رضایی کهخایی[1]، پاپادوپولو لامبرینی[2]

۱. گروه پترولوژی و زمین شناسی اقتصادی، دانشکده علوم زمین، دانشگاه صنعتی شاهرود، ایران
۲. گروه کانی‌شناسی پترولوژی و زمین شناسی اقتصادی، دانشکده زمین شناسی، دانشگاه آریستوتل، یونان

اطلاعات مقاله

تاریخ ارسال: ۲۰۲۵/۰۲/۰۵
تاریخ داوری: ۲۰۲۵/۰۴/۲۱
تاریخ پذیرش: ۲۰۲۵/۰۵/۲۶

DOI: 10.22044/jme.2025.15713.3020

کلمات کلیدی

زمین دمافشارسنجی
شیمی کانی
گرانیتوئید
گودحوض
کرمان

چکیده

استوک گرانیتوئیدی ژوراسیک زیرین گودحوض (180±1.5 Ma) به عنوان بخشی از پهنه دگرگونی-ماگمایی سنندج-سیرجان (SSMMZ) واقع در جنوب شرقی ایران به درون دگرگونی‌های پالئوزوئیک بالایی و سنگ‌های آذرین-رسوبی تریاس نفوذ کرده است. این توده از سه واحد سنگی اصلی شامل دیوریت، گرانودیوریت و گرانیت/آلکالی فلدسپار گرانیت تشکیل شده است و با مقادیر کمتری از گابرو همراهی می‌شود. این استوک، اساساً از گرانیتوئیدهای با بافت دانه‌ای متوسط تا درشت دانه متشکل از کلینوپیروکسن، آمفیبول، بیوتیت، پلاژیوکلاز، آلکالی فلدسپار و کوارتز تشکیل شده است. کلینوپیروکسن‌ها دارای ترکیب کلسیک از دیوپسید تا اوژیت و سالیت هستند، درحالی که آمفیبول‌ها از نوع کلسیک، عمدتاً با ترکیب هورنبلند به عنوان فاز کانیایی اصلی می‌باشند. فلدسپار، تغییرات ترکیبی از ارتوکلاز و الیگوکلاز تا لابرادوریت نشان می‌دهد. شواهد کانی‌شناسی و ژئوشیمیایی بیانگر آن است که ماگمای گرانیتی سازنده توده از نوع I و کالکوآلکالن بوده و در یک محیط کمان ماگمایی حاشیه فعال قاره تشکیل شده است و دارای پتانسیل مس- طلا می‌باشد. برآوردهای زمین دمافشارسنجی براساس کلینوپیروکسن (دمای ۸۰۰ تا ۱۳۰۰ درجه سانتی‌گراد و فشار ۱۲ تا ۴/۵ کیلوبار)، آمفیبول (دمای ۷۴۲ تا ۷۶۹ درجه سانتی‌گراد و فشار ۲ تا ۴/۵ کیلوبار)، و بیوتیت (دمای ۵۸۹ تا ۸۷۵ درجه سانتی‌گراد و فشار ۰/۴۵ تا ۲/۲۷ کیلوبار) بیانگر وجود سه مخزن ماگمایی متفاوت برای انباشت و ذخیره‌سازی ماگما در اعماق پوسته قاره‌ای زیرین (عمق ۴۵ کیلومتری)، میانی (عمق ۱۵ کیلومتری) و بالایی (عمق ۵ کیلومتری) در یک جایگاه کمان قاره‌ای فعال در تریاس پسین- ژوراسیک پیشین در بخش جنوب شرقی پهنه دگرگونی ماگمایی سنندج-سیرجان در جنوب شرقی ایران است.

نویسنده مسئول مکاتبات: h-ghasemi@shahroodut.ac.ir (ح. قاسمی)